ORIGINAL ARTICLE

Pancreatic lipase-related protein 2 is selectively expressed by peritubular myoid cells in the murine testis and sustains long-term spermatogenesis

Hai-Ping Tao[1,2,3] · Teng-Fei Lu[4] · Shuang Li[1,2,3] · Gong-Xue Jia[1,2,3] · Xiao-Na Zhang[1,2,3] · Qi-En Yang[1,2,3] [iD] · Yun-Peng Hou[4]

Abstract

Spermatogenesis is a complicated process of germ cell differentiation that occurs within the seminiferous tubule in the testis. Peritubular myoid cells (PTMCs) produce major components of the basement membrane that separates and ensures the structural integrity of seminiferous tubules. These cells secrete niche factors to promote spermatogonial stem cell (SSC) maintenance and mediate androgen signals to direct spermatid development. However, the regulatory mechanisms underlying the identity and function of PTMCs have not been fully elucidated. In the present study, we showed that the expression of pancreatic lipase-related protein 2 (*Pnliprp2*) was restricted in PTMCs in the testis and that its genetic ablation caused age-dependent defects in spermatogenesis. The fertility of *Pnliprp2* knockout animals *(Pnliprp2$^{-/-}$)* was normal at a young age but declined sharply beginning at 9 months. *Pnliprp2* deletion impaired the homeostasis of undifferentiated spermatogonia and severely disrupted the development and function of spermatids. Integrated analyses of single-cell RNA-seq and metabolomics data revealed that glyceride metabolism was changed in PTMCs from *Pnliprp2$^{-/-}$* mice. Further analysis found that 60 metabolites were altered in the sperm of the *Pnliprp2$^{-/-}$* animals; notably, lipid metabolism was significantly dysregulated. Collectively, these results revealed that *Pnliprp2* was exclusively expressed in PTMCs in the testis and played a novel role in supporting continual spermatogenesis in mice. The outcomes of these findings highlight the function of lipid metabolism in reproduction and provide new insights into the regulation of PTMCs in mammals.

Hai-Ping Tao, Teng-Fei Lu and Shuang Li have contributed equally to this work.

✉ Qi-En Yang
yangqien@nwipb.cas.cn

✉ Yun-Peng Hou
hou@cau.edu.cn

1 Key Laboratory of Adaptation and Evolution of Plateau Biota, Northwest Institute of Plateau Biology, Chinese Academy of Sciences, Xining 810008, Qinghai, China

2 University of Chinese Academy of Sciences, Beijing 100049, China

3 Qinghai Key Laboratory of Animal Ecological Genomics, Northwest Institute of Plateau Biology, Chinese Academy of Sciences, Xining 810001, Qinghai, China

4 State Key Laboratory of Farm Animal Biotechnology Breeding, College of Biological Sciences, China Agricultural University, Beijing 100193, ChinaExtended author information available on the last page of the article

Graphical abstract
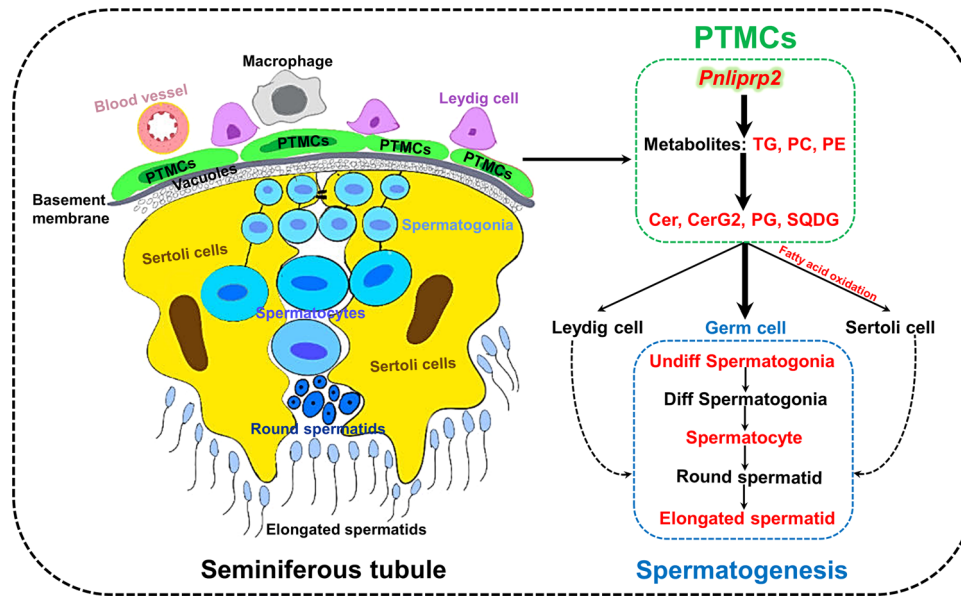
Introduction

Spermatogenesis is a coordinated process of germ cell differentiation that relies on regulatory signals from testicular somatic cells [1]. Peritubular myoid cells (PTMCs) enclose the seminiferous tubules in the testis and act as the major contributor of the basement membrane that creates a unique microenvironment for spermatogenic cells [2]. PTMCs play essential roles in spermatogenesis by providing structural integrity to the seminiferous tubule, contracting to transport spermatozoa, and secreting key regulatory factors [3–5]. PTMCs and Sertoli cells secrete proteins and other substances to form the basal lamina in the testis [6]. These two somatic cell populations supply niche factors that promote the maintenance of spermatogonial stem cells (SSCs) and metabolize retinol to direct spermatogonial differentiation [7–10]. In addition, PTMCs are targets of androgen signaling that is indispensable for spermatid differentiation and fertility [11]. Understanding the genetic mechanisms underlying the development and function of PTMCs is of great significance for tackling fertility problems in males.

PTMCs are smooth muscle-like cells that originate from a mesenchymal stem cell population in the embryonic gonad, which also gives rise to fetal Leydig cells. The formation of PTMCs and Leydig cell lineages relies on multiple signaling pathways, including Wingless-related integration site (Wnt) [12], Desert hedgehog (Dhh) [13], and Platelet-derived

growth factor (Pdgf) [14]. These factors are likely derived from Sertoli cells because the identities of differentiated PTMCs and Leydig cells are lost upon induced depletion of Sertoli cells in neonatal testes [15]. The fate-specification of PTMCs is marked by the expression of smooth muscle alpha (α)-2 actin (Acta2) and myosin heavy chain 11 (Myh11) [16]. At the transcriptional level, PTMCs contain two clusters with distinctive molecular signatures [12]. Only a limited number of genes have been identified to be specific to PTMCs in the testis. For example, the transcriptional repressor hypermethylated in cancer 1 (Hic1) is expressed in a proportion of PTMCs in the neonatal testis, and its deletion causes dilation of seminiferous tubules in mice [17]. The G protein-coupled receptor Lgr4 is selectively expressed in PTMCs and is essential for meiosis progression in mice [18]. Despite these important findings, our understanding of this cell type is still incomplete compared to germ cells and other somatic lineages in the testis.

Pancreatic lipase-related protein 2 (Pnliprp2) is a triglyceride lipase, and its expression was originally identified in the pancreas [19] and in enterocytes of the small intestine [20]. Unlike its closely related family member Pnliprp1, Pnliprp2 possesses lipase activity that can catalyze the hydrolysis of galactose ester [21], phospholipid [22], and retinyl ester [23, 24]. *Pnliprp2* expression is transiently increased in the pancreas of newborns, and its genetic ablation causes problems with absorption and digestion of milk fat in suckling pups. Interestingly, *Pnliprp2*-deficient mice
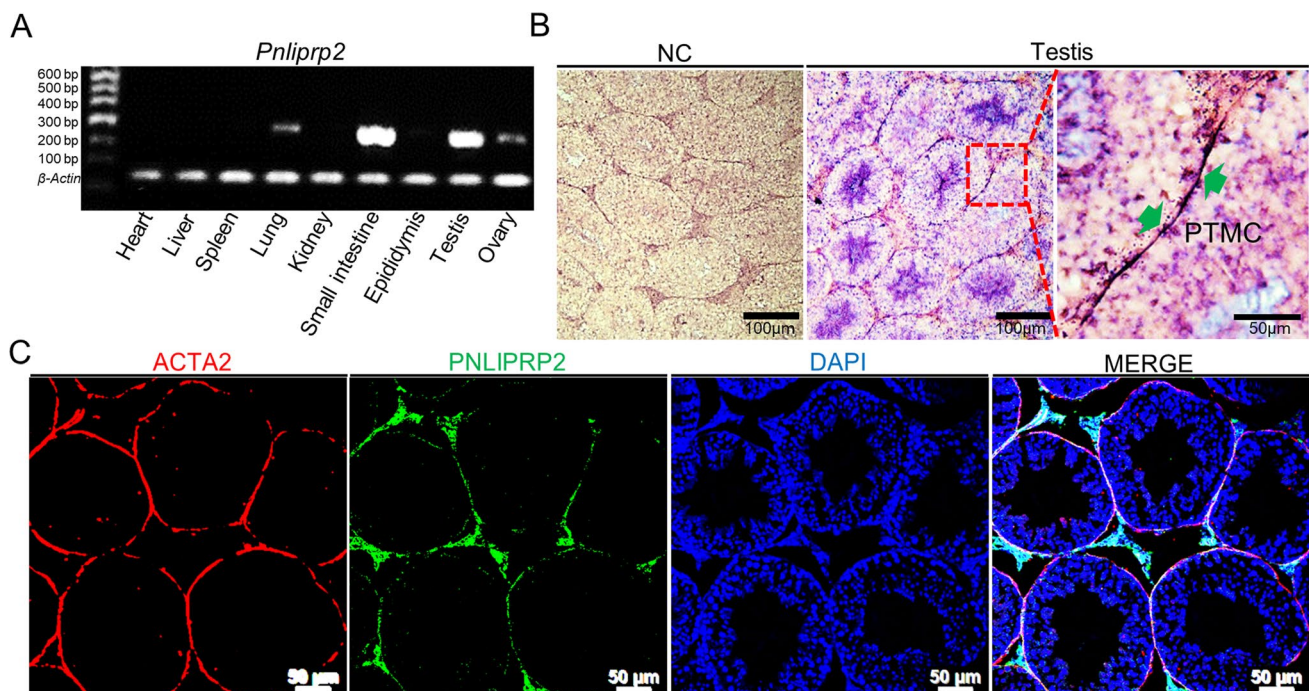
Fig. 1 Relative mRNA expression and protein localization of PNLIPRP2 in PTMCs. **A**. *Pnliprp2* mRNA was expressed in different tissues. From left to right, the collected tissues were the heart, liver, spleen, lung, kidney, small intestine, epididymis, testis and ovary. The total template volume was 1 μg. *β-Actin* was used as a loading control for total RNA; **B**. Localization of PNLIPRP2 in testis. A single strand of DNA that was complementary to the hybridization in situ probe and labeled with digoxin was used as a negative control. The green arrow indicates *Pnliprp2*-positive cells after color rendering. Scale bars = 100 μm; local magnification scale bars = 50 μm; *NC* negative control. **C**. Representative images of immunofluorescent costaining of PNLIPRP2 and ACTA2. Scale bars = 50 μm; green fluorescence is PNLIPRP2; ACTA2 marks peritubular myoid cells (PTMCs) with red fluorescence; blue fluorescence marks the nucleus of DAPI

show normal fat absorption after weaning [25]. It is worth noting that the expression of Pnliprp2 is not restricted to the pancreas and intestine in adult animals, and this gene likely has important actions in a tissue-specific manner under specific physiological or pathological conditions. Pnliprp2 expression is induced in the liver of mice after feeding a vitamin A-deficient diet or in cytotoxic T cells after interleukin stimulation [23, 26]. Several lines of evidence have indicated that Pnliprp2 may play functional roles in reproduction. Pnliprp2 protein is enriched in developing oocytes, and its downregulation affects egg hatching in an insect species [27]. In goats, Pnliprp2 is present and displays enzyme activities (lipase and phospholipase) that can hydrolyze triglycerides, oleic acid and other fatty acids in semen [28]. Pnliprp2 expression is associated with testosterone levels [28]; however, its localization and function in the testis remain unclear.

In the present study, we showed that Pnliprp2 was specifically expressed in PTMCs in mouse testes. Using a *Pnliprp2* knockout line, we demonstrated that Pnliprp2 regulates spermatogenesis in an age-dependent mechanism. Histological, single-cell transcriptomic and metabolomic analyses revealed that *Pnliprp2* deletion severely affected function and gene expression of PTMC in the testis. Consequently,

homeostasis of the undifferentiated spermatogonial lineage was affected, and spermatid development was disrupted. Taken together, our study adds to the understanding of the molecular mechanism of *Pnliprp2* and confirms the important role of PTMCs in spermatogenesis and testicular function.

Results

Relative mRNA expression and protein localization of PNLIPRP2 in PTMCs

First, we examined the expression and abundance of *Pnliprp2* mRNA in various tissues of 8-week-old mice using qRT−PCR. Previous studies identified *Pnliprp2* expression in at least two tissues: pancreas and small intestine [20, 26]. Our results showed that transcripts were also highly expressed in the testes of adult mice (Fig. 1A). We then examined the presence and cellular localization of *Pnliprp2* mRNA in the testis using in situ hybridization (ISH). Tissues from the small intestine were used as a positive control (Supplemental Fig. 1A). *Pnliprp2*-positive cells were spindle-shaped cells surrounding the seminiferous tubules (Fig. 1B),
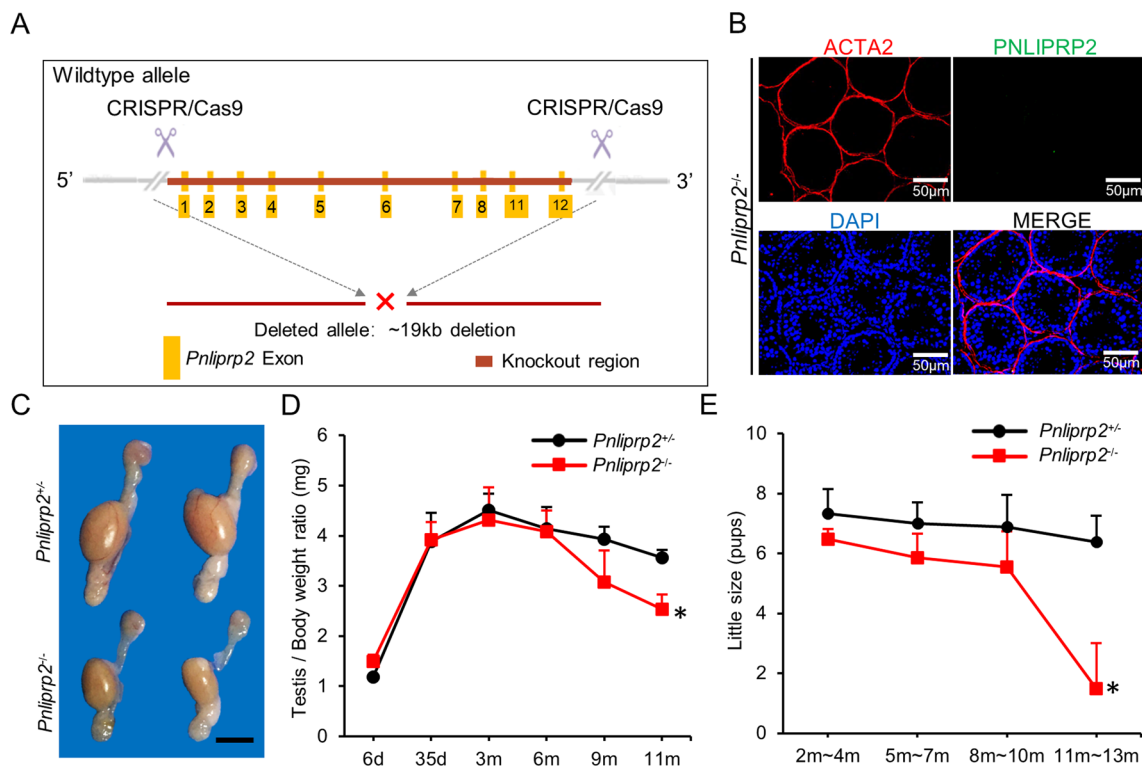
Fig. 2 *Pnliprp2* deletion leads to age-dependent fertility loss. **A**. Schematic diagram of *Pnliprp2⁻ᐟ⁻* mice generated by using CRISPR/ Cas9 technology. **B** Knockout efficiency was identified at the protein level, and green fluorescence was PNLIPRP2. ACTA2 marked peritubular myoid cells with red fluorescence. Scale bar = 50 μm. **C** The testes and epididymis of 9-month-old *Pnliprp2⁺ᐟ⁻ and Pnliprp2⁻ᐟ⁻* mice. **D** Testis/body weight of *Pnliprp2⁻ᐟ⁻* and *Pnliprp2⁺ᐟ⁻* mice at 6 days, 35 days, 3 months, 6 months, 9 months and 11 months (n = 3). (E) Quantification of the average litter size of *Pnliprp2⁺ᐟ⁻* and *Pnliprp2⁻ᐟ⁻* male mice (n = 3)

indicating that this gene was likely specifically expressed in the cells around the basement membrane. Immunofluorescence (IF) staining of PNLIPRP2 and ACTA2, which marks PTMCs in the testis, revealed that these two proteins were colocalized (Fig. 1C). Together, these data revealed that the *Pnliprp2* transcript was exclusively present in PTMCs in the testis.

Pnliprp2 deletion leads to age-dependent fertility loss and spermatogenic defects

Next, we examined the function of *Pnliprp2* in spermatogenesis using a knockout approach. Because an efficient *Cre* mouse line that specifically targets the PTMC lineage in the testis is not available [29, 30], we generated a global *Pnliprp2* knockout model (*Pnliprp2⁻ᐟ⁻*) using CRISPR/Cas9 technology (Fig. 2A). Genotyping results showed that *Pnliprp2* was successfully deleted, and IF staining failed to detect its expression in PTMCs in the testes of *Pnliprp2⁻ᐟ⁻* male mice (Fig. 2B and Supplemental Fig. 1B–D). The knockout mice were born at the expected Mendelian ratio and developed normally after reaching adulthood (Supplemental Fig. 1E, F). While *Pnliprp2⁻ᐟ⁻* females exhibited normal fertility and

ovarian function (Supplemental Fig. 2), the males displayed an age-dependent decline in fertility with reduced testis size (Fig. 2C–E and Supplemental Fig. 1G). Specifically, we noticed that the testis weight of *Pnliprp2⁻ᐟ⁻* began to decline at 9 months of age (Supplemental Fig. 1G). Although the body weight was similar between adult *Pnliprp2⁻ᐟ⁻* and littermate controls (Supplemental Fig. 1F), the testis to body weight ratio was reduced by 21.8% at 9 months (3.94 ± 0.25 *vs.* 3.08 ± 0.63, $P = 0.27$) and by 31.3% at 11 months (3.62 ± 0.12 *vs.* 2.54 ± 0.30, $P < 0.05$) compared to littermate controls (Fig. 2D). The fertility test revealed that the litter sizes of knockout and control mice were comparable at 4 months but decreased at 6 months of age and continued to decline at 9 and 11 months. At 11 months of age, the average litter size of the *Pnliprp2⁻ᐟ⁻* males was only 1.5, which was significantly different from the 6.39 litter size of the controls (n = 3, $P < 0.05$) (Fig. 2E).

To determine the reason for reduced fertility, we conducted histological analysis on cross-sections from testes of 1-, 3-, 6-, 9-, and 11-month-old control and *Pnliprp2⁻ᐟ⁻* mice. H&E staining revealed that seminiferous tubules of control animals contained completed spermatogenesis; in sharp contrast, spermatogenesis in *Pnliprp2⁻ᐟ⁻* testis was severely disrupted
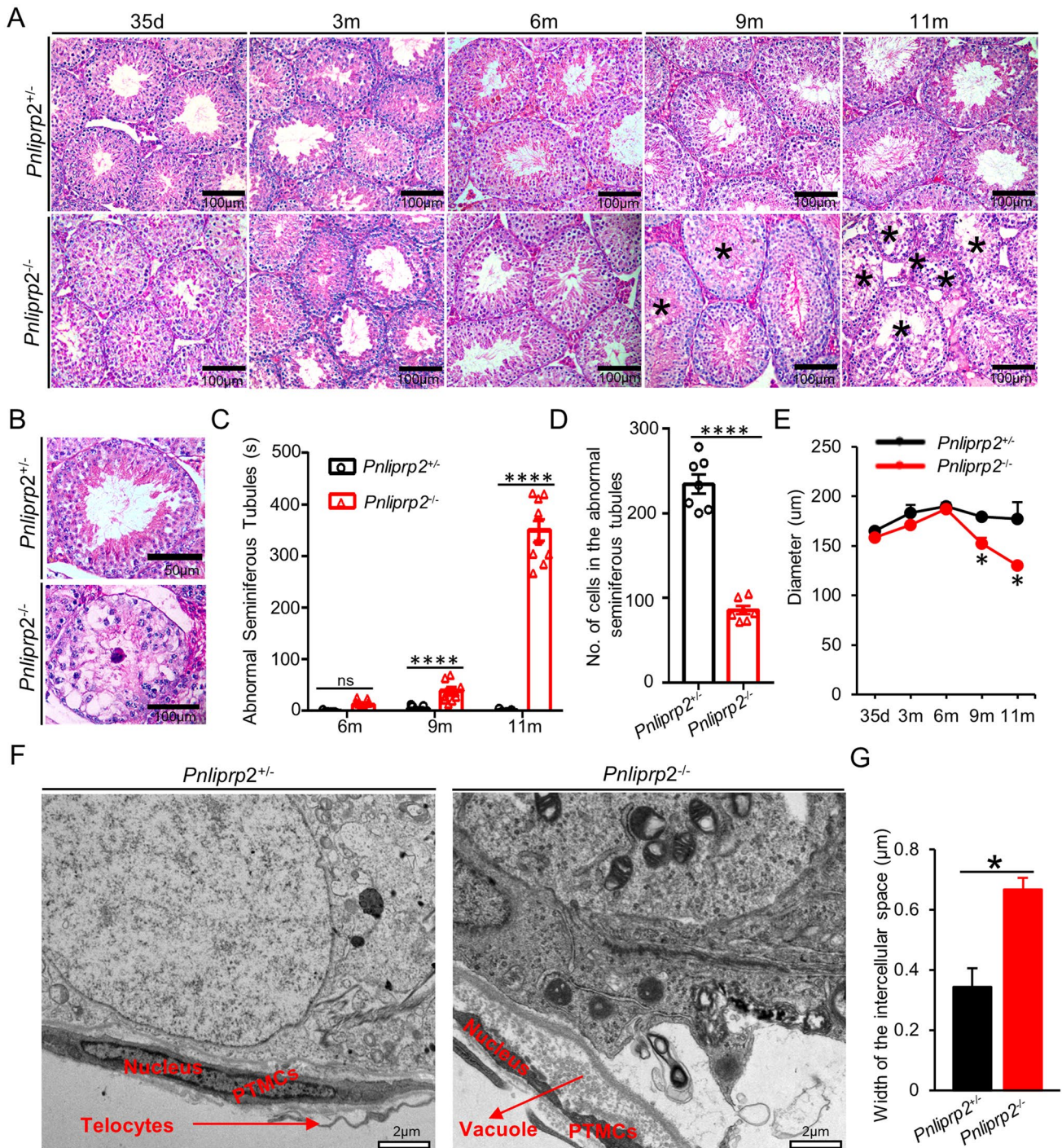
Fig. 3 *Pnliprp2* deletion in PTMCs leads to testicular structure and spermatogenic defects. **A** Representative images of hematoxylin and eosin (H&E)-stained testicular cross-sections of *Pnliprp2⁻/⁻* and *Pnliprp2⁺/⁻* mice at 35 days, 3, 6, 9, and 11 months. Scale bar = 100 μm. **B** Representative images of abnormal seminiferous tubules of *Pnliprp2⁻/⁻* mice at 11 months. Scale bar = 50 μm, 100 μm. **C** Statistical analysis of abnormal seminiferous tubules from 6 to 11 months. n = 3, 500 seminiferous tubules were counted in each group, ****$P < 0.0001$. **D** Number of cells in the abnormal seminiferous tubules. ****$P < 0.0001$ **E** Statistical diagram of spermatogenic tubule diameter (n = 3). Three sections were used for each mouse, and 100 seminiferous tubules were used for diameter measurement. *$P < 0.05$. **F** Representative TEM images of testis PTMCs. Scale bar = 2 μm. **G** Statistical analysis of the width of the intercellular space from PTMCs. n = 3, 5 TEM images were counted in each sample, *$P < 0.05$
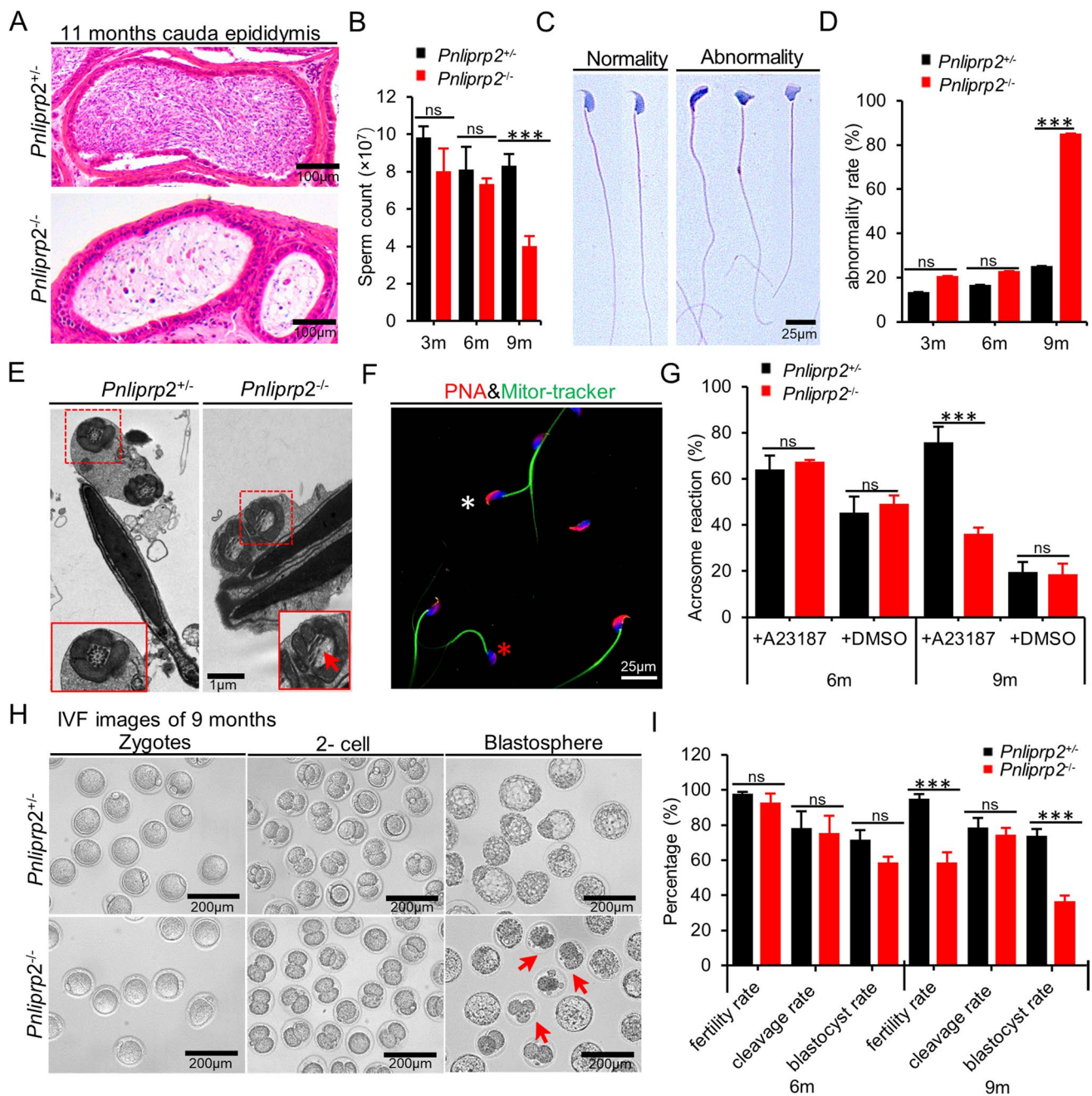
Fig. 4 *Pnliprp2* deletion affected spermatid development and sperm function. **A** H&E staining of 9-month cauda epididymides in *Pnliprp2*$^{-/-}$ and *Pnliprp2*$^{+/-}$ mice. Scale bars = 100 μm. **B** Sperm count of *Pnliprp2*$^{-/-}$ and *Pnliprp2*$^{+/-}$ mice at 3, 6 and 9 months. ***$P < 0.001$. **C** H&E images of normal and abnormal sperm. Scale bars = 25 μm. **D** Abnormality rate of *Pnliprp2*$^{-/-}$ and *Pnliprp2*$^{+/-}$ mice at 3, 6 and 9 months. ***$P < 0.001$. **E** Representative TEM images of epididymal sperm from 9-month-old *Pnliprp2*$^{-/-}$ and *Pnliprp2*$^{+/-}$ mice. Scale bars = 5 μm. (F-G) Representative images

F and rate **G** of acrosome reaction (AR) induced by A23187 from 9-month-old sperm in *Pnliprp2*$^{-/-}$ and *Pnliprp2*$^{+/-}$ mice. At least 800 sperm were counted for each genotype. Scale bars = 25 μm, White *indicates no AR, and red *indicates AR, ***$P < 0.001$, n = 3. (H) Representative images of IVF from *Pnliprp2*$^{-/-}$ and *Pnliprp2*$^{+/-}$ mice at 9 months. Scale bars = 200 μm. (I) Fertilization, cleavage and blastocyst rates of *Pnliprp2*$^{-/-}$ and *Pnliprp2*$^{+/-}$ mice at 6 and 9 months. ***$P < 0.001$, n = 3

at 11 months with disorganized spermatogenic cells and the presence of vacuoles (Fig. 3A). Detailed analysis revealed that the affected tubules contained a smaller number of spermatogonia, spermatocytes and misoriented spermatids (Fig. 3B,

D). Spermatogenic defects did not appear in the testes of *Pnliprp2*$^{-/-}$ males at 6 months of age; however, the diameter of seminiferous tubules was marginally decreased at 9 months of age (179.51 μm ± 1.84 μm *vs.* 152.35 μm ± 5.74 μm,

$P < 0.05$). The number of abnormal seminiferous tubules was significantly increased (Fig. 3C, E). A total of 7.86% of seminiferous tubules contained detectable abnormal spermatogenesis at 9 months (3.19 ± 1.68 *vs.* 39.3 ± 6.54, $P < 0.001$), and this number was increased to 70.09% at 11 months (1.47 ± 1.01 *vs.* 350.30 ± 20.76, $P < 0.001$) (Fig. 3C). The seminiferous epithelial cycle was also disordered at this stage. For example, the percentage of seminiferous tubules in stages IV-VI was increased ($21.45 \pm 2.02\%$ *vs.* $29.92 \pm 1.96\%$, $P < 0.05$), while the percentage of tubules in stages VII-VIII was decreased ($39.27\% \pm 1.95\%$ *vs.* $33.42\% \pm 0.72\%$, $P < 0.05$) (Supplemental Fig. 3). The testis structure was further analyzed by TEM (transmission electron microscope), and normal PTMCs surrounded the outer layer of the basement membrane of the seminiferous tubules, with flat or elongated cells. The cytoplasm contained abundant mitochondria and a smooth endoplasmic reticulum, and there was a layer of telocytes (TCs) with beaded protrusions on the outer layer. Compared with the controls, the *Pnliprp2*$^{-/-}$ animals had significantly deformed PTMC nuclei, condensed cytoplasm, and significant vacuoles in the cytoplasm. In addition, the intercellular space was significantly broadened (Fig. 3F, G). TEM analysis of spermatocytes revealed a coarse meshwork of nuclear chromatin in spermatocytes, and some spermatocytes from knockout mice exhibited necrosis with vacuoles at the cytoplasmic rim, exacerbated mitochondrial swelling, and nuclear envelope dissolution (Supplemental Fig. 4A, B). The Sertoli cell structure of the *Pnliprp2*$^{-/-}$ animals was still normal, but the density of the cytoplasm was reduced (Supplemental Fig. 4C, D). Together, these data suggested that spermatogenesis was disrupted by *Pnliprp2* deletion; as a result, fertility declined in an age-dependent manner.

Pnliprp2 deletion affected spermatid development and sperm function

To dissect the reasons for the reduced fertility, we measured the concentration, morphology, and fertilization capacity of sperm from control and *Pnliprp2*$^{-/-}$ mice. Compared with the controls, the sperm concentration of *Pnliprp2*$^{-/-}$ animals was significantly reduced at 9 months of age (8.32×10^7 *vs.* 4.00×10^7, $P < 0.001$) (Fig. 4A, B), while the number of abnormal sperm reached 85.23% ($25.32\% \pm 4.85\%$ *vs.* $85.23\% \pm 4.56\%$, $P < 0.001$) (Fig. 4C, D). TEM analysis of sperm ultrastructure showed broken microtubule structures and mitochondrial myelin sheaths in sperm from *Pnliprp2*$^{-/-}$ mice (Fig. 4E). We also found that the sperm motility of *Pnliprp2*$^{-/-}$ mice was impacted. The occurrence of the acrosome reaction (AR) was assessed using the ionophore A23187, which induces calcium influx in sperm and ARs [31]. At 6 months, the incidence of

spontaneous and induced ARs was similar; however, the incidence of induced ARs in *Pnliprp2*$^{-/-}$ mice decreased significantly ($75.89 \pm 6.64\%$ *vs.* $36.22 \pm 2.69\%$, $P < 0.01$) at 9 months (Fig. 4F, G). The in vitro fertilization results further confirmed that *Pnliprp2* deletion affected the cleavage rate ($58.67 \pm 5.81\%$ *vs.* $94.95 \pm 2.54\%$, $P < 0.01$) and blastocyst rate ($36.65 \pm 3.17\%$ *vs.* $73.88 \pm 3.89\%$, $P < 0.01$) of sperm from *Pnliprp2*$^{-/-}$ mice (Fig. 4H, I). We also examined meiotic progression using spermatocyte nuclear spreading, and the results indicated that the percentages of germ cells in leptotene, zygotene, pachytene, diplotene and diakinesis were similar in the testes of *Pnliprp2*$^{-/-}$ and control animals, indicating that meiosis progression was not impacted by *Pnliprp2* deletion (Supplementary Fig. 5). Taken together, these observations indicated that *Pnliprp2* deficiency impacted sperm quantity and function, therefore causing a decline in fertility.

Pnliprp2 function is crucial for sustaining the undifferentiated spermatogonial lineage

Because we noticed that the total number of spermatogenic cells was reduced in *Pnliprp2*$^{-/-}$ mice as early as 9 months of age, we next examined whether the homeostasis of the spermatogonial lineage that contains the foundational SSCs and progenitor spermatogonia was influenced in these mice (Fig. 3D). Quantification of the germ cell/Sertoli cell ratio using immunofluorescence co-staining of the germ cell marker TRA98 and the Sertoli cell marker SOX9 revealed that the number of germ cells decreased in *Pnliprp2*$^{-/-}$ mice at 9 months (6098.43 ± 440.78 *vs.* 4422.58 ± 145.23, $P < 0.05$) (Fig. 5A and D). It appeared that germ cell loss was not a result of elevated apoptosis because the results of the terminal deoxynucleotidyl transferase dUTP nick end labeling (TUNEL) assay revealed no difference in apoptosis of testicular cells from control and knockout mice from 3 to 11 months of age (Fig. 5C and F). Importantly, the overall number of undifferentiated spermatogonia, which were labeled by LIN28A expression, was significantly decreased by 29.47% (0.65 ± 0.01 *vs.* 0.46 ± 0.03, $P < 0.01$) and 20.54% (0.57 ± 0.01 *vs.* 0.45 ± 0.03, $P < 0.05$) in the testes of 9- and 11-month-old *Pnliprp2*$^{-/-}$ mice, respectively (Fig. 5B and E).

To further determine the fate decisions of undifferentiated spermatogonia, we examined the proliferation and ratio of A_{single} (A_s), A_{paired} (A_{pr}), and $A_{aligned}$ (A_{al}) spermatogonial subtypes (Fig. 6A). Whole mount staining of seminiferous tubules for LIN28A revealed a significant increase in A_s spermatogonia (26.51 ± 2.87 *vs.* $63.35\% \pm 7.86\%$, $P < 0.05$) and a significant reduction in A_{al} spermatogonia ($43.08\% \pm 2.67\%$ *vs.* $16.70\% \pm 6.85\%$, $P < 0.05$) at 11 months
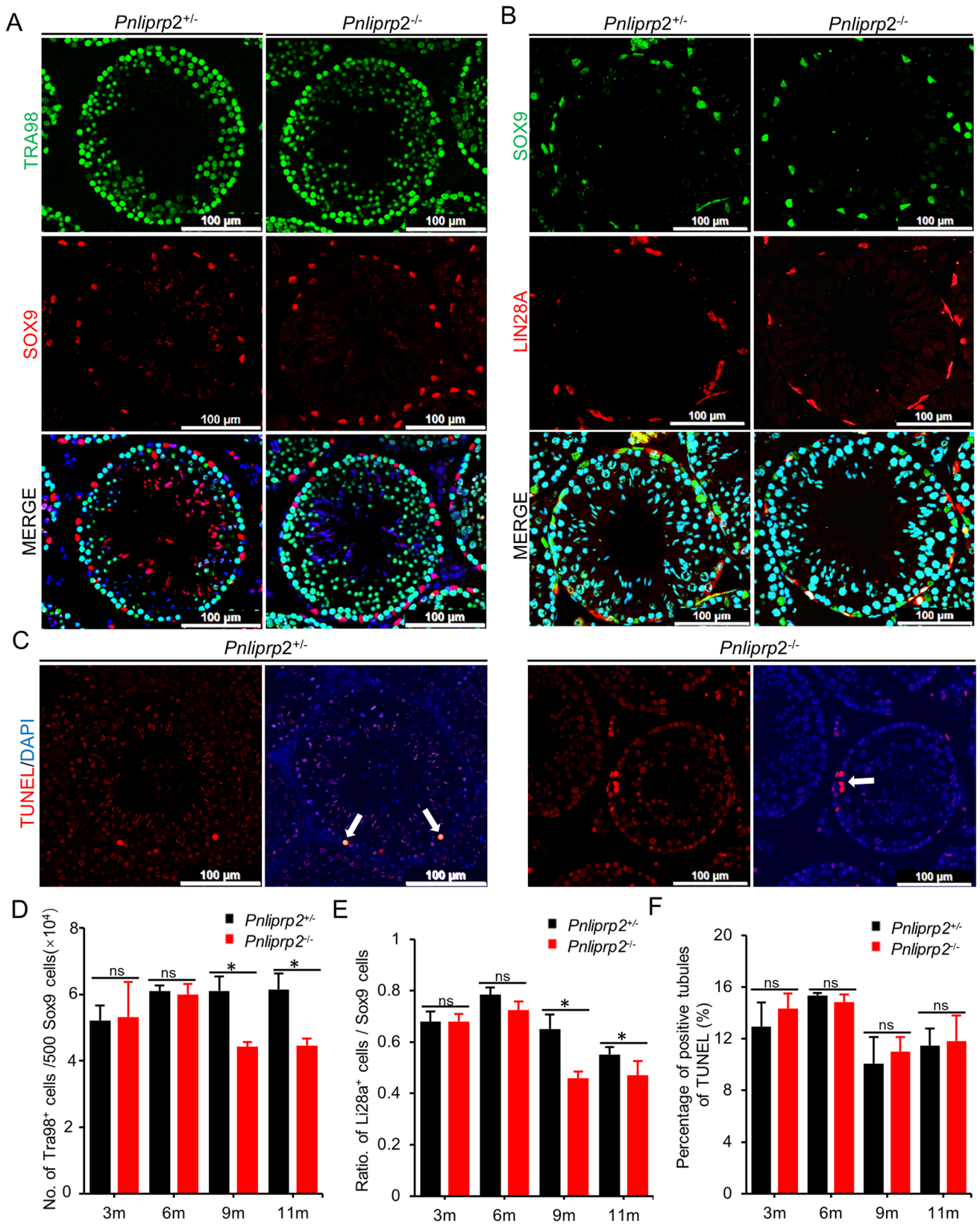
◄ **Fig. 5** *Pnliprp2* function is important for the maintenance of undifferentiated spermatogonia. **A** Immunofluorescence with SOX9 (red, the marker of Sertoli cells), TRA98 (green, the marker of germ cells) and DAPI (blue) in *Pnliprp2*$^{-/-}$ and *Pnliprp2*$^{+/-}$ mouse testes. Scale bars = 100 μm. **B** Immunofluorescence staining for LIN28A (red, a marker of undifferentiated spermatogonia), SOX9 (green, a marker of Sertoli cells) and DAPI (blue) in *Pnliprp2*$^{-/-}$ and *Pnliprp2*$^{+/-}$ mouse testes. Scale bars = 50 μm. **C** Immunofluorescence staining for TUNEL (red) and DAPI (blue) in *Pnliprp2*$^{-/-}$ and *Pnliprp2*$^{+/-}$ mouse testes. Scale bars = 100 μm. **D** Statistics of the number of TRA98$^+$ cells per 500 SOX9$^+$ cells in *Pnliprp2*$^{-/-}$ and *Pnliprp2*$^{+/-}$ mice at 3, 6, 9 and 11 months. At least 1500 SOX9$^+$ cells were counted from 3 mice of each genotype. *P < 0.05. **E** Quantifications of LIN28A$^+$ cells/SOX9$^+$ cells in *Pnliprp2*$^{-/-}$ and *Pnliprp2*$^{+/-}$ mouse testes at 3, 6, 9, and 11 months. At least 1500 SOX9$^+$ cells were counted for 3 mice of each genotype. **P < 0.01. **F** Statistics of the number of apoptotic cells in the testes of *Pnliprp2*$^{-/-}$ and *Pnliprp2*$^{+/-}$ mice at 3, 6, 9 and 11 months

of age (Fig. 6B). Next, we labeled proliferative spermatogonia using an EdU incorporation assay, and the results showed that LIN28A$^+$ A$_{s,}$ A$_{pr}$ and A$_{al}$ spermatogonia with EdU and retention rates in LIN28A$^+$ spermatogonia were significantly increased in *Pnliprp2*$^{-/-}$ mice compared to controls (A$_s$: 13.17 ± 9.52% *vs.* 42.67 ± 4.35%, P < 0.05; A$_{pr}$: 13.58 ± 7.45% *vs.* 47.91% ± 5.62%, P < 0.05; A$_{al}$: 73.25 ± 16.78% *vs.* 25.04 ± 2.31%, P < 0.05) (Fig. 6C). IF staining of c-Kit, which marks differentiating spermatogonia within the seminiferous tubules, showed that the number of differentiating spermatogonia did not change significantly (Supplementary Fig. 6). We then examined the expression of genes related to SSC fate decisions in PTMCs and spermatogonia cocultured cells as described previously [5]. Isolated PTMCs were positive for ACTA2, and interestingly, Oil Red O staining revealed that *Pnliprp2*-deficient PTMCs appeared to contain enriched lipid contents (Fig. 7A, B). Thy1$^+$ testicular cells from wild-type pups were then cocultured with PTMCs from control or *Pnliprp2* knockout mice for 3 days. The results of Ki67 and LIN28A staining showed that the percentage of proliferative undifferentiated spermatogonia was reduced in *Pnliprp2*-deficient PTMC cultures (Fig. 7C, D). The relative expression of *Lin28a* and *Ddx4* did not change significantly, but *Id4* was decreased by 73%, while *Bcl6b* was increased by 412% in spermatogonia cultured with *Pnliprp2*$^{-/-}$ PTMCs (Fig. 7E). The results revealed that the ability of PTMCs to support gene expression associated with SSC maintenance was altered by *Pnliprp2* deletion. Furthermore, the mRNA levels of *Nppb* (natriuretic peptide type B, quiescence factors of contraction) and *Agt* (angiotensinogen, stimulators of PTMC contraction) were significantly elevated in PTMCs isolated from *Pnliprp2* knockout animals (Fig. 7F) [32], indicating that genes regulating contraction were also impacted. Collectively, these data indicated that the deletion of *Pnliprp2* impacted the homeostasis of undifferentiated spermatogonia and changed the expression of genes associated with SSC fate decisions.

Pnliprp2 deletion changed gene expression and the developmental trajectory in PTMCs

Single-cell RNA-seq analysis is a powerful method to reveal dynamics in gene expression and the developmental trajectory of testicular cells [33]. We isolated testicular cells from 2-month-old control and *Pnliprp2*$^{-/-}$ mice and examined gene expression at single-cell resolution using the 10 × Genomics platform. A total of 13,800 *Pnliprp2*$^{+/-}$ and 13,318 *Pnliprp2*$^{-/-}$ testicular cells passed standard quality control and were retained for subsequent analysis. We selected highly variable genes and performed principal component analysis (PCA) and hierarchical clustering on the significant principal components. Twenty cell clusters were obtained by combining *Pnliprp2*$^{+/-}$ and *Pnliprp2*$^{-/-}$ testicular cells (clusters C0 to C19) (Fig. 8A, Supplementary Fig. 7). Expression enrichment of known markers and differentially expressed genes (DEGs) (Fig. 8B, C) allowed us to assign the identity of the cell clusters. We identified spermatogenic cells at various developmental stages (expressing *Ddx4*, *Dazl*, *Stra8*, *Sycp1* or *Tnp1*) and three main somatic cell populations, including Sertoli cells (expressing *Ar*), Leydig cells (expressing *Hsd3b1*), and PTMCs (expressing *Acta2*) (Supplementary Fig. 8A-B). A total of 21, 66, 424 and 39 DEGs were identified in germ cells, Sertoli cells, and Leydig cells, respectively (Supplementary Fig. 8C). We selected DEGs to detect their mRNA expression levels in spermiogenesis, such as *Odf1* (outer dense fiber of sperm tails 1), *Capza3* (capping actin protein of muscle Z-line subunit alpha 3), *Sun5* (Sad1 and UNC84 domain containing 5), and *Rdh11* (retinol dehydrogenase 11), and found that their expression levels were significantly reduced (Supplementary Fig. 8D and Table S4). Because *Pnliprp2* was specifically expressed in PTMCs, this cell fraction was extracted from whole testicular cells using previously identified marker genes (*Acta2* and *Myh11*). The extracted cells were assigned into 3 subclusters (Fig. 8D, E), indicating that the PTMCs contained three distinct fractions at the single-cell level. *Pnliprp2* expression was downregulated in all these cells in *Pnliprp2*$^{-/-}$ mice compared to controls (Fig. 8H); however, its deletion did not affect the proportion of cells in these three clusters. Further analysis showed that a total of 25 genes were downregulated and 14 genes were upregulated in the PTMCs of *Pnliprp2*$^{-/-}$ mice These DEGs were functionally enriched in the cGMP-PKG signaling pathway, glycolipid metabolism, protein processing in the endoplasmic reticulum, and the oxytocin signaling pathway (Fig. 8F). We selected DEGs to detect their mRNA expression level in the glycolipid metabolism pathway, such as *Dgkh* (diacylglycerol kinase), *Fdft1* (farnesyl diphosphate farnesyl transferase 1) and *Pdxdc1* (containing pyridoxine-dependent decarboxylase domain 1), and found that their expression level was significantly reduced (Fig. 8G and Table S4). Cell
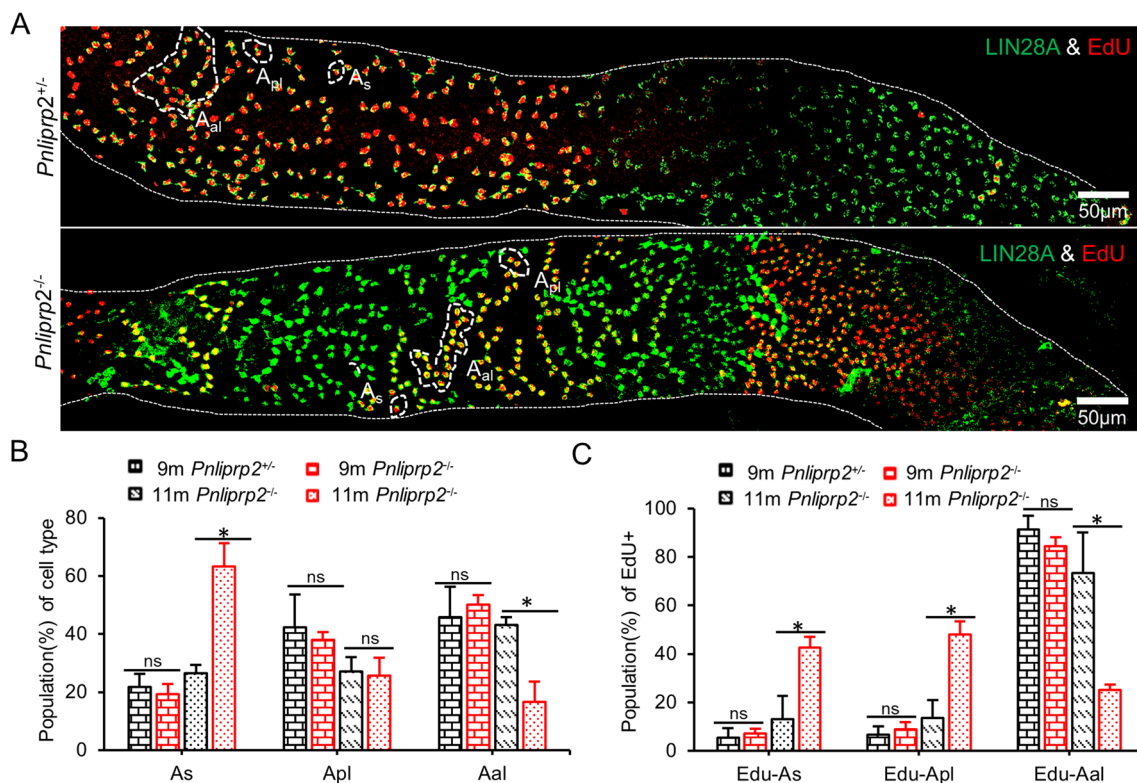
Fig. 6 *Pnliprp2* function is crucial for fate decisions of undifferentiated spermatogonial population. **A** Images of EdU (red, the marker of cell proliferation) and LIN28A (green, the marker of undifferentiated spermatogonia) by whole-mount staining in *Pnlilprp2*$^{-/-}$ and *Pnliprp2*$^{+/-}$ seminiferous tubules at 9 and 11 months after EdU injection. Scale bars = 50 μm. **B**, **C** Proportions of A$_s$, A$_{pr}$ and A$_{al}$ spermatogonia proportions with or without EdU in LIN28A$^+$ cells in *Pnliprp2*$^{-/-}$ and *Pnliprp2*$^{+/-}$ mice. At least 1000 LIN28A$^+$ cells were counted from 3 mice of every genotype, *$P < 0.05$

communication among cell types using CellChat demonstrated that PTMCs intensively communicated with germ cells, Leydig cells and Sertoli cells (Fig. 8I). Together, the outcomes of these experiments showed that loss of *Pnliprp2* function impacted the gene expression of PTMCs and likely affected germ cells indirectly.

Pnliprp2 deletion altered the developmental trajectory and gene expression in undifferentiated spermatogonial subtypes

Because PTMCs showed strong communication with germ cells, we next focused on spermatogonia to reveal the impact of *Pnliprp2* loss of function on putative SSCs and progenitor spermatogonia. Reclustered germ cells contained 10 different clusters (Fig. 9A), and the expression of genes enriched in the spermatogonia compartment was enriched in cluster 6 (Fig. 9A, B). Pseudotime trajectory analysis revealed that cells from Cluster 6 were at the beginning of the trajectory, further supporting this conclusion (Fig. 9C, D). Three different states were identified among these spermatogonial cells (SPG0-2), and trajectory analysis indicated that SPG0 was the initial cell population (Fig. 9E, F). Quantitatively, we determined that 18.6%, 35.2%, and 46.2% of cells sorted into SPG0, SPG1 and SPG2, respectively, in the *Pnliprp2*$^{+/-}$ sample and 14.6%, 51.8% and 33.6% of cells sorted into SPG0, SPG1 and SPG2, respectively, in the *Pnliprp2*$^{-/-}$ sample (Fig. 9G, H). A dramatic decrease in the percentage of SPG2 cells in the *Pnliprp2*$^{-/-}$ sample suggests that *Pnliprp2* deficiency severely impairs germline stem cell development. A total of 261 DEGs were identified in these three cell lines, including 132 upregulated genes and 129 downregulated genes (Supplementary Fig. 9A). These data indicated that oxidative phosphorylation, pyruvate metabolism and glucose metabolism were enhanced, while glycolysis/gluconeogenesis, cellular senescence and tight junctions were inhibited in spermatogonia upon *Pnliprp2* deletion (Supplementary Fig. 9B). We selected DEGs to detect their mRNA expression levels in the oxidative phosphorylation pathway, such as *Ndufa4* (mitochondrial complex associated) and *Cox7b* (cytochrome c oxidase subunit 7b), and found that their expression levels were significantly reduced (Supplementary Fig. 8E and Table S4).
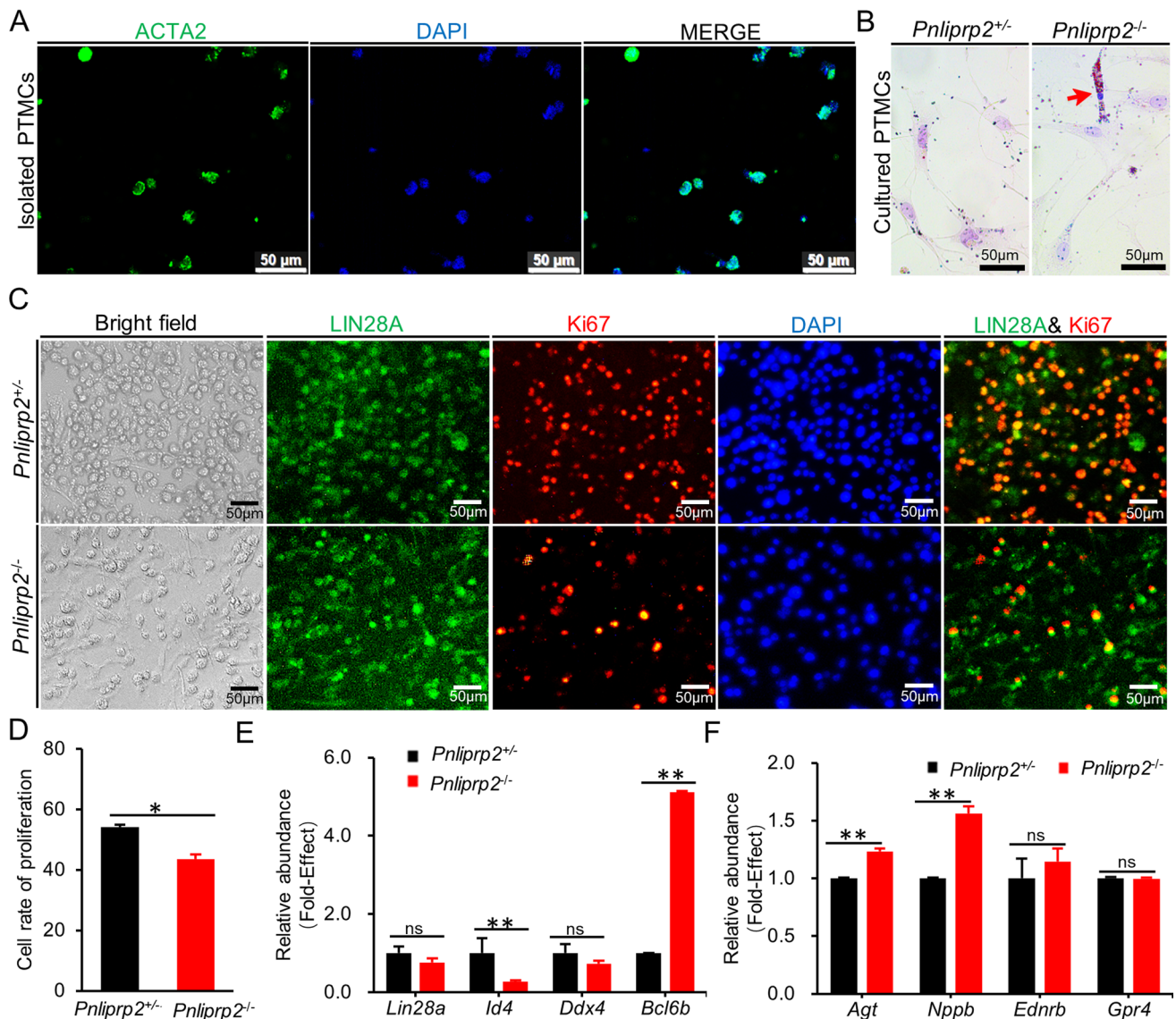
Fig. 7 *Pnliprp2* in PTMCs influences proliferation and gene expression of undifferentiated spermatogonia. **A** Representative image of isolated cells stained with the PTMC marker ACTA2 (green signals). Nuclei were stained with DAPI. Cell purity greater than 80%. Scale bar, 50 μm. **B** Representative image of primary cultured PTMCs by Oil Red O staining, lipid droplets in the cytoplasm of PTMCs (indicated by the red arrow). Scale bar, 50 μm. **C** Representative image of PTMC and SSC cocultured cells. The initial SSC cell count is 2×10^6, LIN28A (green, the marker of undifferentiated spermatogonia) and Ki67 (red, the marker of cell proliferation). **D** Cell ratio of proliferation of SSCs. **indicates a significant difference at $P < 0.01$. **E** qRT–PCR analysis of *Id4, Bcl6b, Lin28a* and *Ddx4* transcript abundance in PTMC and SSC coculture cells. n = 3. **indicates a significant difference at $P < 0.01$. ns: indicates no difference. **F** The mRNA levels of genes implicated in smooth muscle contraction, such as *Nppb*, *Gpr4*, *Ednrb*, and *Agt,* in isolated PTMCs of *Pnliprp2^−/−^* and *Pnliprp2^+/−^* mice

The functions of Sertoli cells and Leydig cells were impacted in *Pnliprp2^−/−^* mice

Because PTMCs showed strong communication with Sertoli cells and Leydig cells, we next focused on somatic cells to reveal the impact of *Pnliprp2* loss of function on Sertoli cells and Leydig cells. Reclustered Sertoli cells contained 7 different clusters (Fig. 10A). Compared with those in *Pnliprp2^+/−^* mice, Sertoli cells in *Pnliprp2^−/−^* mice

were distributed in each cluster. A total of 66 DEGs were identified in these three cell subtypes, including 34 upregulated genes and 32 downregulated genes (Fig. 10B). Differential gene analysis showed that upregulated DEGs were enriched in lipid metabolism (Fig. 10C). We selected DEGs to detect their mRNA expression level in the ether lipid metabolism pathway, such as *Alad* (Aminolevulinate, delta-, dehydratase), *Plb1* (Phospholipase b1*)* and *Cd2 bp2* (CD2 cytoplasmic tail binding protein 2), and found that
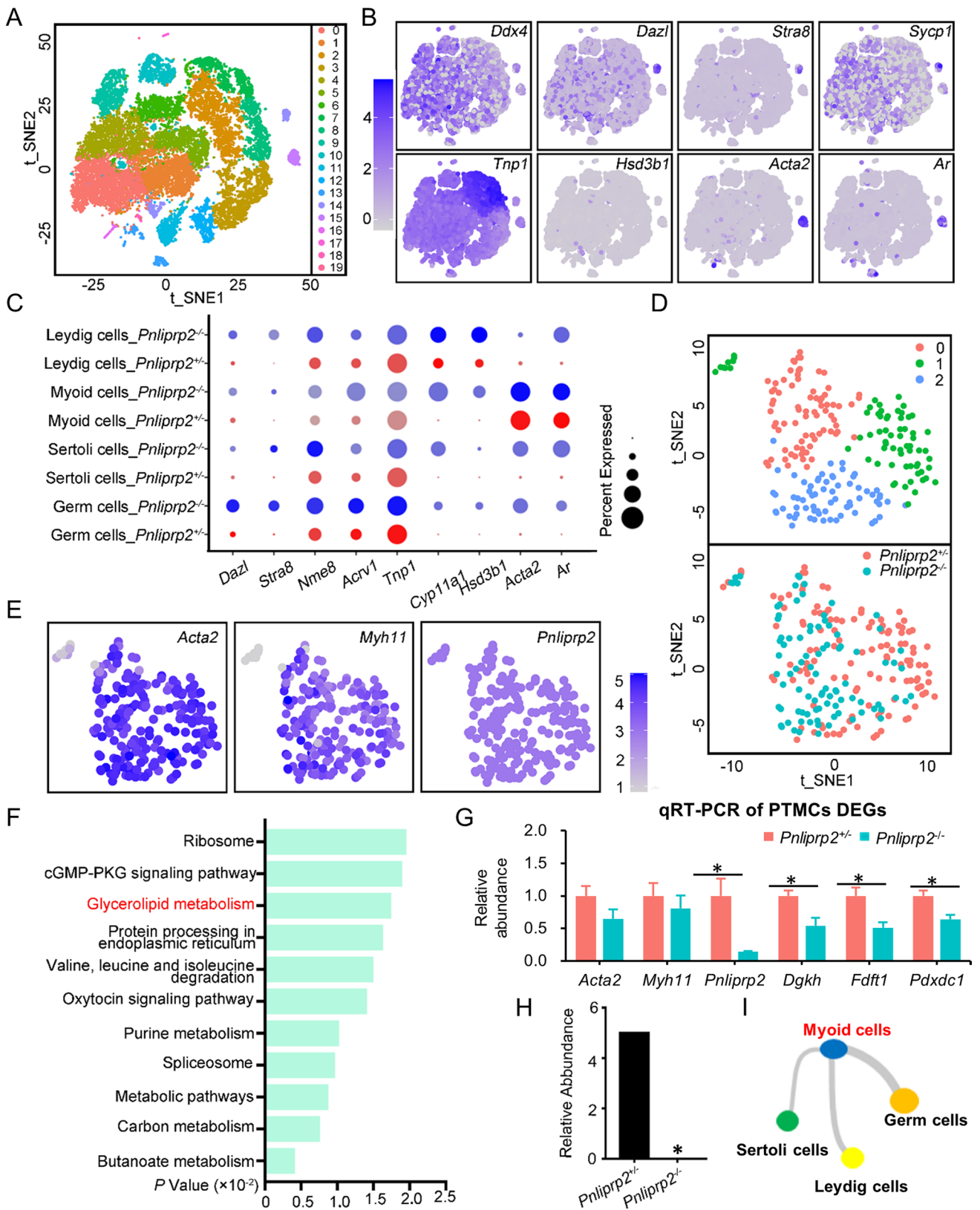
◄**Fig. 8** *Pnliprp2* deletion changed gene expression and the developmental trajectory in PTMCs. **A** t-SNE and clustering analysis of combined single-cell transcriptome data from *Pnliprp2⁻/⁻* and *Pnliprp2⁺/⁻* testicular single cells. Each dot represents a single cell, and cell clusters are distinguished by colors. **B** Gene expression patterns of selected germ cell and somatic cell marker genes projected on the t-SNE plots; **C** Dotplot for expression of selected marker genes across all identified cell types in *Pnliprp2⁻/⁻* and *Pnliprp2⁺/⁻* testicular cells; **D** Focused analysis (t-SNE clustering) of combined (Top), *Pnliprp2⁻/⁻* and *Pnliprp2⁺/⁻* (Bottom) myoid cells documented 3 biological subtypes. **E** Expression pattern of myoid cell marker genes in t-SNE of myoid cells. **F** The FPKM in *Pnliprp2⁻/⁻* compared with *Pnliprp2⁺/⁻* myoid cells. **G** Compared with *Pnliprp2⁺/⁻* myoid cells, *Pnliprp2⁻/⁻* regulated triglyceride metabolism was consistent with the function of PNLIPRP2 hydrolase and consistent with the results of lipid metabolism. **H** qRT−PCR analysis of PTMC marker genes and DEGs of the glycerolipid metabolism pathway. $*P < 0.05$. **I** There was cell signal communication between myoid cells and other cell types

their expression levels were significantly increased (Supplementary Fig. 8D and Table S4).

Cell communication among different cell types was analyzed by CellChat, and Sertoli cells communicated strongly with germ cells and Leydig cells, and this communicating signal was altered by PNLIPRP2 deletion (Fig. 8I). Next, reclustered Leydig cells contained 2 different clusters (Fig. 10E). Similar to Sertoli cells, Leydig cells in *Pnliprp2⁻/⁻* mice were distributed in both clusters compared with controls (Fig. 10E). Further analysis showed that 194 genes were downregulated and 230 genes were upregulated in the Leydig cells of *Pnliprp2⁻/⁻* mice (Fig. 10F). These DEGs were functionally enriched in the mitochondrial protein catabolic process, tetrapyrrole biosynthetic process and cAMP signaling pathway (Fig. 10G). We selected DEGs to detect their mRNA expression level in the metabolism pathway, such as *Ndufa4l2* (Mitochondrial complex associated like 2) and *Cox7a2l* (Cytochrome c oxidase subunit 7A2 like), and found that their expression levels were significantly reduced (Fig. 10H Table S4). However, we did not find changes in testosterone levels (Supplementary Fig. 1H). Taken together, these data suggested that age-related dysregulation of spermatogenesis was closely related to the diminishing metabolic function of Sertoli cells and Leydig cells.

Pnliprp2 deletion altered the lipid metabolome in the testis

In scRNA-seq, we discovered that glycolipid metabolism was downregulated in PTMCs from *Pnliprp2⁻/⁻* mice, leading to the retardation of spermatogonial proliferation and thereby affecting spermatogenesis. Next, we conducted metabolomics analysis to screen the candidate molecules that mediate the actions. To this end, untargeted lipidomics analysis was performed on the testes from the controls ($n = 7$) and the *Pnliprp2⁻/⁻* samples ($n = 7$). After stringent

quality control (Supplemental Fig. 10 and Supplemental Fig. 11), 60 metabolites were detected to be significantly different between the controls and *Pnliprp2⁻/⁻* mice. Of these, 37 metabolites were upregulated, while 23 metabolites were downregulated (Fig. 11A), such as phosphatidyl choline (PC), phosphatidyl ethanolamine (PE) and triglyceride (TG) (Fig. 11B). Research findings have shown that testis maturation, germ cell development and sperm function are related to lipid composition. Phospholipids (PLs), especially PC and PE, are major integral components of plasma membranes and are also involved in sperm membrane permeability and fluidity [34, 35] and acrosomal reactions [36]. Asymmetry of phospholipids and their fatty acids in the sperm inner and outer plasma membranes greatly influences epididymal maturity [37] and sperm motility [38]. Long-chain fatty acid TG metabolism disorder impairs male fertility [39]. These findings and research further confirmed that abnormal lipid metabolism is the reason for the decrease in sperm acrosome occurrence and fertilization rate in *Pnliprp2⁻/⁻* mice. Pathway analysis with MetaboAnalyst 5.0 showed the involvement of multiple metabolites connected to metabolism. Specifically, many metabolites were significantly enriched in signaling pathways, including the triacylglycerol signaling pathway and prostaglandin signaling pathway (Fig. 11C, D). The significantly upregulated metabolites were ceramides (Cer), diglycosylceramide (CerG2), phosphatidylglycerol (PG) and sulfoquinovosyldiacylglycerol (SQDG) (Fig. 11E). Free fatty acids are mainly stored in lipid droplets in the form of triacylglycerol. Testicular lipid droplets are mainly distributed in Leydig cells and Sertoli cells. Subsequently, we selected some genes related to lipid metabolism and verified their expression in testicular tissue through qRT−PCR. We found that the mRNA expression level of the gene *Lipe* (Lipase E, hormone sensitive type) related to glycerol metabolism was significantly reduced, while the expression level of *Gk* (Glycerol kinase) was significantly increased. The expression levels of *Fabp3* (fatty acid binding protein 3) and *Cpt2* (carnitine palmitoyl transferase 2) genes related to fatty acid metabolism were significantly reduced. *StAR* (steroidogenic acute regulatory protein) and *Hsd17b12* (hydroxysteroid (17-beta) dehydrogenase 12) regulate cholesterol synthesis, and their expression levels were significantly reduced (Fig. 11F). We further measured the concentrations of the highly expressed metabolites triglyceride (TG) and ceramide (Cer) in the testis and PTMCs by ELISA and found that their expression levels increased significantly (Fig. 11G). In summary, these data suggested that ablation of *Pnliprp2* leads to an increase in the relative content of triacylglycerol and that elevated testicular triglycerides are associated with abnormal expression of key enzymes involved in triacylglycerol synthesis (Rosiglitazone [40], Acylglycerolphosphate acyltransferase [41]), hydrolysis (Adipose triglyceride lipase [39], Hormone sensitive lipase [42]) and
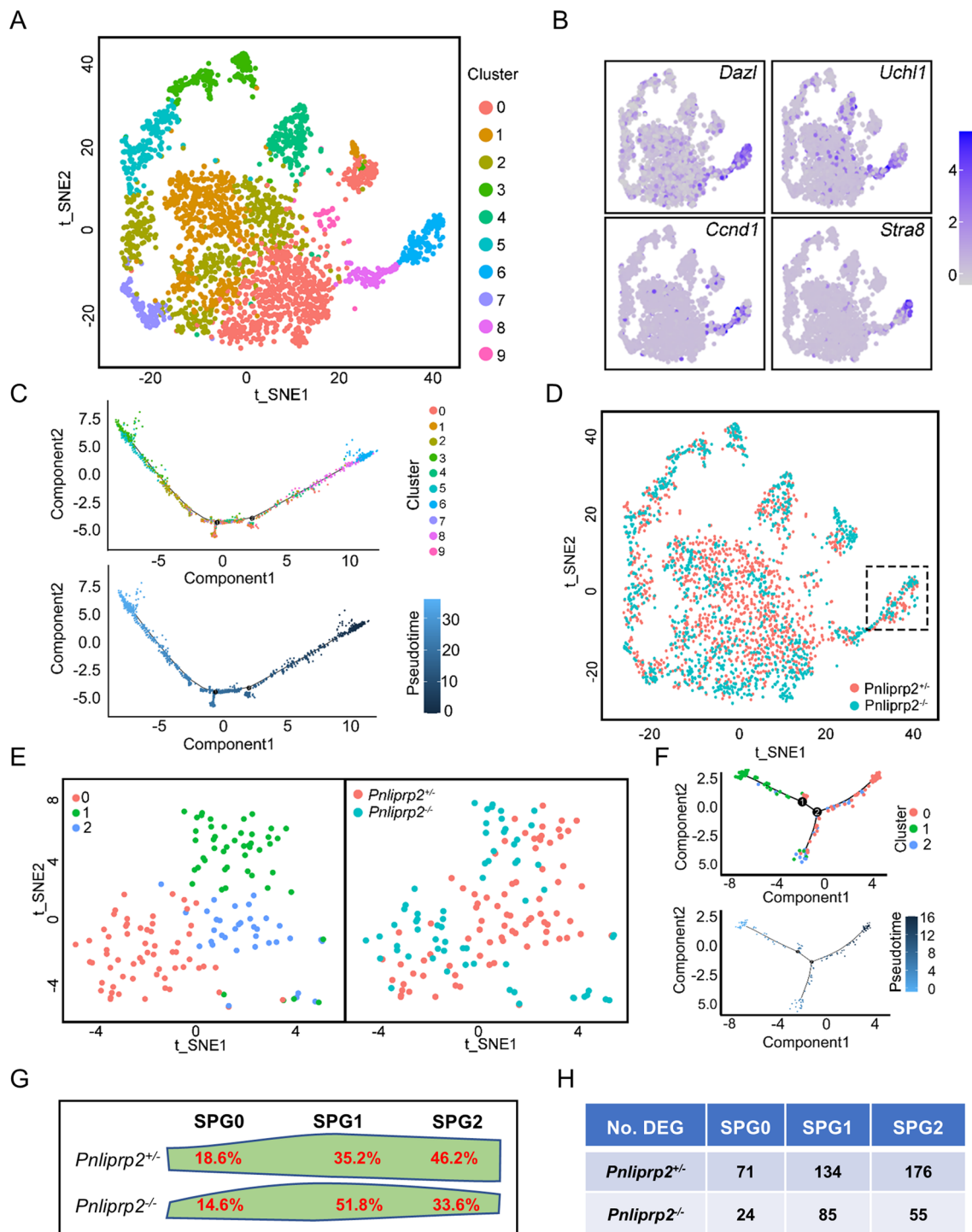
Fig. 9 *Pnliprp2* deletion altered spermatogonial fate decisions and gene expression. **A** Focused t-SNE clustering analysis of combined germ cells. Germ cells documented 10 biological subtypes. Each dot represents a single cell, and cell clusters are distinguished by colors. **B** Gene expression patterns of selected marker genes corresponding to spermatogonia in germ cells and concentrated in clusters 6 and 8. **C** Pseudotime ordering of combined germ cells by monocle2, clus-

ter6 were developmental origin subpopulation. **D** *Pnliprp2⁻/⁻* and *Pnliprp2⁺/⁻* germ cells in early reproductive development. The spermatogonia fraction is circled. **E** Spermatogonia were reclustered and analyzed in combination in a t-SNE diagram. **F** Spermatogonia were divided into 3 states: state 0-state 1-state 2. **G-H** Different developmental state proportions of *Pnliprp2⁻/⁻* and *Pnliprp2⁺/⁻* spermatogonia
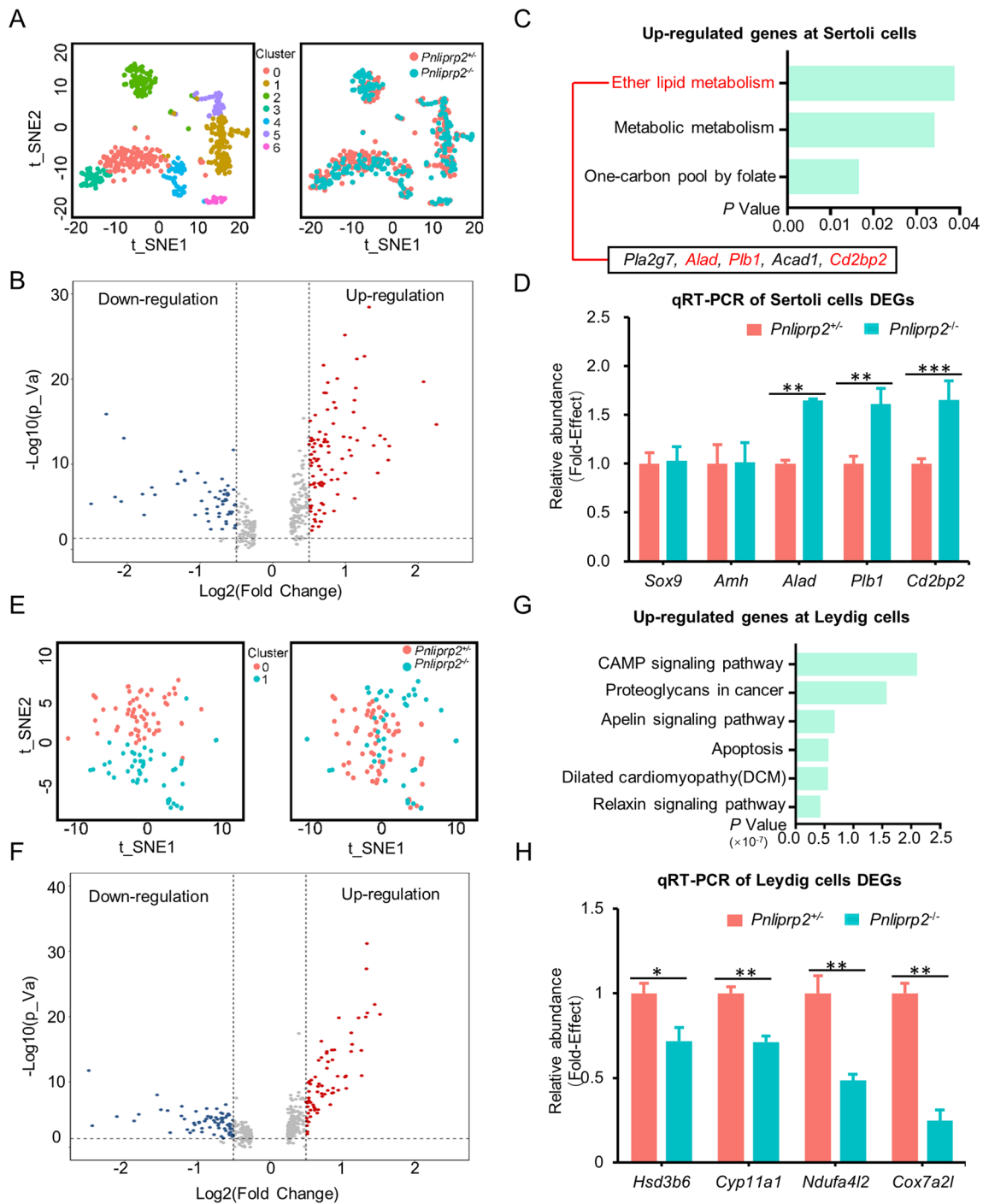
Fig. 10 The function of Sertoli cells and Leydig cells was impacted in *Pnliprp2⁻/⁻* mice. **A** t-SNE and clustering analysis of combined single-cell transcriptome data from *Pnliprp2⁻/⁻* and *Pnliprp2⁺/⁻* Sertoli cells. Each dot represents a single cell, and cell clusters are distinguished by colors. **B** Scatterplots of differentially expressed genes in Sertoli cells. Red scatter, genes with significant upregulation; blue scatter, genes with significant downregulation; gray scatter, genes with no significant difference. **C** Upregulated gene enrichment in KEGG pathway analysis, *Pla2g7, Alad, Plb1, Acad1* and *Cd2 bp2* genes enriched in ether lipid metabolism. The genes highlighted in red are used for verification. **D** qRT−PCR analysis of Sertoli cell marker genes and DEGs of the ether lipid metabolism KEGG path-way. **P < 0.01, ***P < 0.001. **E** t-SNE and clustering analysis of combined single-cell transcriptome data from *Pnliprp2⁻/⁻* and *Pnliprp2⁺/⁻* Leydig cells. Each dot represents a single cell, and cell clusters are distinguished by colors. **F** Scatterplots of differentially expressed genes in Leydig cells. Red scatter, genes with significant upregulation; blue scatter, genes with significant downregulation; gray scatter, genes with no significant difference. The downregulated genes *Ndufa4l2* and *Cox2a2l* are associated with metabolic pathways. **G** Upregulated gene enrichment in KEGG pathway analysis, genes enriched in the cAMP signaling pathway. **H** qRT−PCR analysis of Leydig cell marker genes and DEGs of the metabolic pathway. *P < 0.05, **P < 0.01
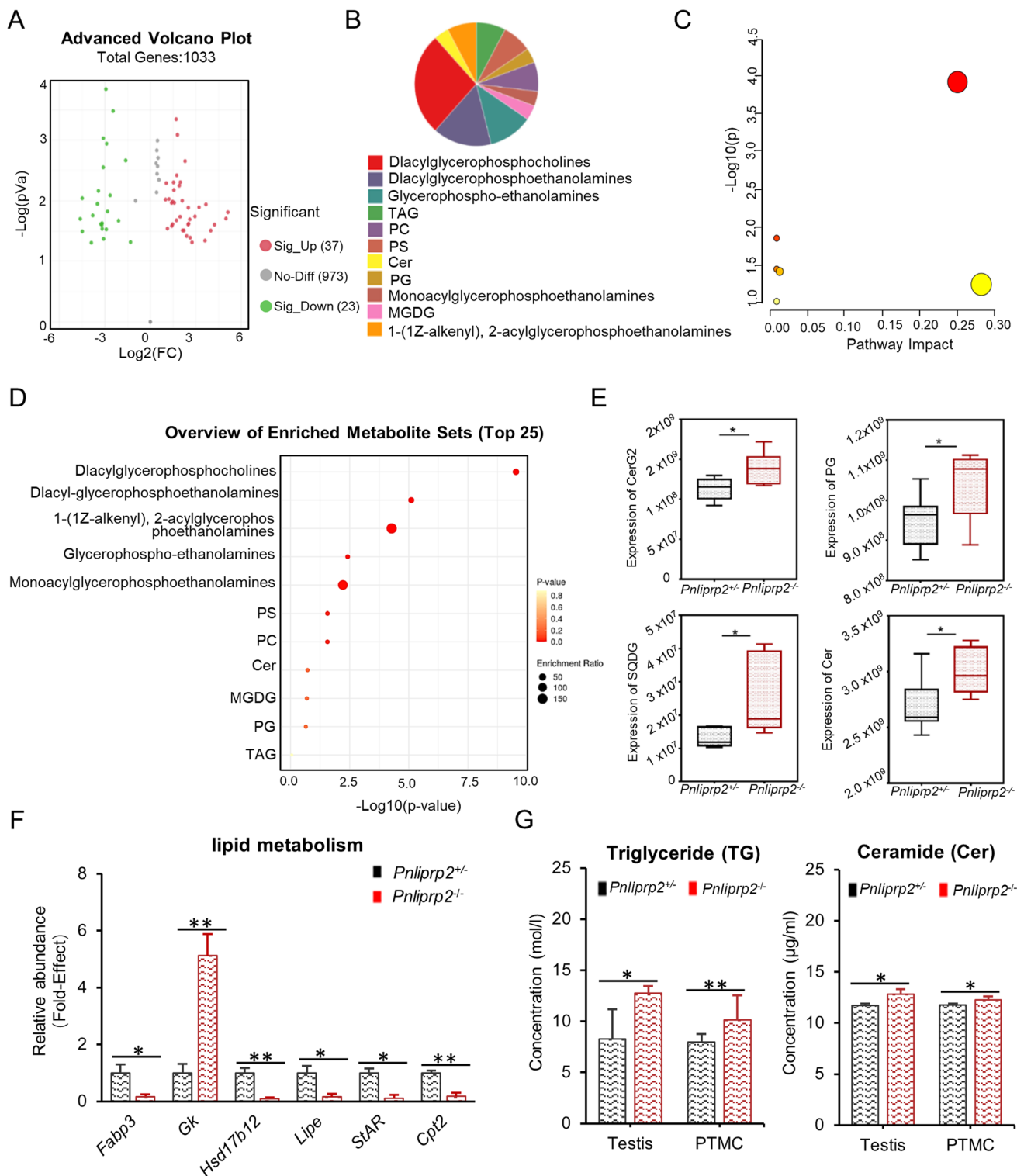
Fig. 11 *Pnliprp2* deletion altered the lipid metabolome in the testis. **A** Volcanic map of differential lipid metabolites. **B** Differential metabolite clustering pie chart. **C** Pathway analysis results of differential metabolites. **D** Analysis of differential lipid metabolite metabolic pathways in control and knockout mice. **E** Box plots showing representative metabolite changes in testes between *Pnliprp2*$^{+/-}$ and *Pnliprp2*$^{-/-}$ mice. **F** The mRNA expression levels of lipid metabolism genes in the testicular tissue of *Pnliprp2*$^{+/-}$ and *Pnliprp2*$^{-/-}$ mice. *$P < 0.05$, **$P < 0.01$. **G** Concentration of triglyceride (TG) and downstream metabolite ceramide (Cer) in testes and PTMCs of *Pnliprp2*$^{+/-}$ and *Pnliprp2*$^{-/-}$ mice. *$P < 0.05$, **$P < 0.01$

lipid droplet formation (Seipin [43]). However, which key genes and key metabolites are involved in the regulation of lipid metabolism awaits further investigation.

Discussion

PTMCs are essential components of the testicular microenvironment and play indispensable roles in directing spermatogenesis in mammalian testes [44]. Here, we discovered a specific role of *Pnliprp2* in supporting PTMC function and long-term maintenance of spermatogenesis. Using ISH and IF staining, we provided strong evidence that *Pnliprp2* expression was restricted to PTMCs in mouse testes. Genetic ablation of *Pnliprp2* impaired spermatogonial fate decisions and sperm function in adult mice. Taken together, these data conclusively establish *Pnliprp2* as an essential factor in the maintenance of the spermatogenic lineage in the testis, which is essential to ensure robust spermatogenesis and male fertility.

A novel finding of this study is that *Pnliprp2* was highly expressed in PTMCs of the testis. Previous studies have identified that *Pnliprp2* is constitutively expressed in the pancreas and epithelial and Paneth cells of the intestine [26, 45]. Under certain conditions, *Pnliprp2* expression is induced in cytotoxic T lymphocytes [46] and the liver [47]. Pancreatic *Pnliprp2* is responsible for dietary fat digestion during the neonatal period of development [25]. Pnliprp2 is localized in PTMCs, and its protein is not distributed in the intercellular space, indicating that *Pnliprp2* is not a secretory protein in the testis, which is different from its expression pattern in the pancreas [25, 26]. Although PTMCs and Leydig cells are derived from common progenitors during early development [16], *Pnliprp2* expression distinguishes these two cell types in the postnatal testis. Liver injury induced the expression of *Pnliprp2* in hepatic stem cells, and interestingly, Acta2 was also stimulated, indicating that the expression of these two genes is correlated [47]. In the testis, the expression of these two genes is specific to PTMCs, and it is possible that a shared transcription program stimulates the expression of a list of genes to support the development and function of PTMCs.

PTMCs have multifaceted roles in directing the fate decisions of undifferentiated spermatogonia. Spermatogenesis mainly contains three major phases: mitosis of spermatogonia, meiosis of spermatocytes and spermiogenesis [48]. Spermatogonia are distributed around the basement membrane and interact closely with PTMCs. A subpopulation of spermatogonia acts as SSCs to sustain long-term spermatogenesis. One of the major roles of PTMCs is to secrete GNDF, which dictates SSC fate decisions and plays an indispensable role in the maintenance of continual spermatogenesis [5]. PTMCs are a source of extracellular matrix

(ECM) proteins, such as fibronectin, collagen, and laminin, to form the basement membrane that serves as an anchor to spermatogonia [49, 50]. In this study, we found that the deletion of *Pnliprp2* did not affect meiosis but severely impacted the homeostasis of spermatogonial populations and the function of spermatids. A dramatic decrease in the percentage of SSCs and progenitor spermatogonia was confirmed by immunohistochemical and scRNA-seq analyses. This phenotype was likely not caused by alteration of niche factors because expression of *Gdnf* and other important niche factors were not modulated by *Pnliprp2* ablation in PTMCs. Instead, DEG analysis indicated that oxidative phosphorylation, pyruvate metabolism and glucose metabolism were upregulated in undifferentiated spermatogonia. The self-renewal of SSCs relies on glycolysis, while spermatogonial differentiation depends on oxidative phosphorylation [51, 52]. We found that inactivation of *Pnliprp2* in PTMCs changed the proportion of A_s spermatogonia and significantly impacted the oxidative phosphorylation process. These findings support the conclusion that changes in lipid metabolism in PTMCs alter metabolic programs in SSCs, therefore affecting the maintenance of this unique germ cell population.

Another finding is that lipid metabolism directed by *Pnliprp2* in PTMCs is crucial for sperm function. Our understanding of the metabolic regulation of spermatogenesis mainly focuses on Sertoli cells, which provide an energy source for developing germ cells [53]. Importantly, the energy of Sertoli cells itself is derived from fatty acid oxidation, and their lipid storage and metabolism are crucial for germ cell survival [53, 54]. In this study, scRNA-seq data revealed that PTMCs intensively communicated with germ cells, Leydig cells and Sertoli cells. Mutual regulation among germ cells, Sertoli cells, PTMCs and Leydig cells is crucial to the construction of the testis and the orderly development of spermatogenesis. Sertoli cells play central roles in sustaining the differentiated state of PTMCs and the differentiation hierarchy of adult Leydig cells in prepubertal testes [15]. In this study, *Pnliprp2* deletion in PTMCs upregulated genes associated with lipid metabolism in Sertoli cells. Terminal differentiation of spermatids is sensitive to alterations in Sertoli cells [55], and we speculated that interactions between Sertoli cells and PTMCs were important for spermatid development and sperm function, which were impaired by *Pnliprp2* in PTMCs. PTMCs and Leydig cells share common progenitors, and these two testicular somatic cells are closely related. *Pnliprp2* deletion did not cause a significant change in testosterone synthesis but affected the transcriptome of Leydig cells and particularly affected genes involved in mitochondrial function. In addition, terminal differentiation and release of sperm is partially regulated by the contractile activities of PTMCs [56], and we found that genes involved in the regulation of the actin cytoskeleton

were changed by *Pnliprp2* deletion. This could lead to the premature release of sperm into the lumen of seminiferous tubules. Collectively, defects in spermatid differentiation and release generated sperm with impaired fertilization capacity in *Pnliprp2*$^{-/-}$ animals.

One limitation of the present study is that we did not study the function of *Pnliprp2* in PTMCs using a conditional knockout approach due to the lack of a specific and efficient Cre tool. However, we have several lines of evidence that strongly support a PTMC-specific role of *Pnliprp2* in spermatogenesis. The primary role of Pnliprp2 in the pancreas and intestine is to digest and absorb milk fat in newborn rodents and humans [57], but its role in fat digestion is dispensable in adult animals [46]. In this study, we found that ablation of *Pnliprp2* did not cause neonatal death or delayed postnatal growth. Furthermore, females lacking *Pnliprp2* function were completely fertile and did not show age-dependent deterioration of ovarian function. Data from culture experiments showed that PTMCs from *Pnliprp2* knockout mice significantly changed the expression profiles of genes related to SSC maintenance and fate decisions. Further studies are required to elucidate the direct effect of PTMCs on the metabolic features of SSCs, Sertoli cells and other somatic lineages in the testis.

Conclusions

In summary, our investigations introduced *Pnliprp2*-dependent lipid metabolism in PTMCs as a crucial component of the SSC niche and a novel regulator of spermatid development in mice. These findings not only provide new insights into the function and regulation of PTMCs but also provide new knowledge on the molecular control of spermatogenesis in general.

Methods

Animals

All mice used in this study were housed in a specific pathogen-free (SPF) environment with enough water and food and regular sunlight following the circadian rhythm of the mice. All animal studies were performed in accordance with guidelines from the Institutional Animal Care and Use of Laboratory Animals and were approved by the Animal Welfare and Ethics Committee at the Northwest Institute, Chinese Academy of Sciences (approval code: hwipb012). Male (C57BL/6 N) mice were purchased from Charles River Laboratory Animal Centre.

CRISPR/Cas9 was used to construct targeted knockout mice by Biocytogen Pharmaceuticals (Beijing) Co., Ltd. Single guide RNAs (sgRNAs) were selected to target the entire coding area of *Pnliprp2* and were as follows: 5′-AGCCTCCCGTACCGCCCACC-3′ and 5′-TGATAA TAACACCCAGCTTA-3′. Briefly, the obtained Cas9/ sgRNA was injected into the fallopian tubes of pseudopregnant female mice to give birth (F0). The edited *Pnliprp2* founders were identified by PCR amplification using the following primers: *Pnliprp2*-F1 5′-TTCCAC CCCTCAAGTGACCAAG-3′; *Pnliprp2*-R1 5′-CATCAG CAGGCTCCACTATTCAC-3′; *Pnliprp2*-F2 5′-GTTCCA CCCCTCAAGTGACCAAG-3′; *Pnliprp2*-R2 5′-GCA ACATCTGCACGGATGGAAAC-3′. Genotypes of the produced mice were identified and sequenced, and two mutant mice were obtained (mice lacking 18,317 bases and 18,313 bases). We selected mice lacking 18,317 bases (F0 *Pnliprp2*$^{+/-}$) and C57BL/6 J mice to cage and bred homozygous individuals (*Pnliprp2*$^{-/-}$) as experimental research objects. The intact allele was 554 base pairs, and the *Pnliprp*2$^{-/-}$ allele was 496 base pairs.

Fertility assay and sperm staining

Forty-five-day-old *Pnliprp2*$^{+/-}$ and *Pnliprp2*$^{-/-}$ male mice were paired with adult wild-type female mice. One male was mated with three females for 12 months. The average number of pups per litter was quantified, and at least three mating cages were set up for each genotype. For sperm count, the epididymis was placed in 1 ml human tubal fluid (HTF) medium and shredded to release sperm. Fifty microliters of sperm suspension was transferred to adhesive slides, spread, dried at room temperature (RT), soaked in methanol, fixed for 10 min, removed, dried, stained with hematoxylin and eosin (H&E), and examined for sperm morphology under a microscope. At least 1500 sperm from three different animals were counted for each group to count the abnormal sperm rate.

Ionophore A23187-induced acrosome reaction (AR)

The AR was evaluated as described previously with modification [58]. Briefly, 1 ml of sperm supernatant suspension was incubated in an incubator (3 °C, 5% CO2) for 1 h for capacitation, and 200 µl of sperm supernatant suspension was removed and divided into two equal parts. One part was treated with 3 µl of 50 µmol/l A23187 (Sigma, C9400-5MG), and the other part was treated with 3 µl of DMSO as a control. After inducing AR for 30 min in an incubator, the sperm suspension was removed, centrifuged at $1000 \times g$ for 5 min to precipitate the sperm, and washed once with PBS. After rinsing in PBS and resuspension, acrosome status was assessed by staining with the acrosome marker peanut

agglutinin (PNA, diluted 1:500) and the mitochondria marker Mito-Tracker (diluted 1:500) at 37 °C for 1 h. After washing three times with PBS, the samples were mounted on slides for immunofluorescence analysis under a Leica DMR Fluorescence Microscope (Mannheim, Germany). The ARs were calculated using the proportion of sperm without intact acrosomes in live sperm with normal nucleus and tails. At least 700 sperm from 3 different animals were counted for each group.

In situ hybridization

The sections were fixed in 4% PFA, conventionally dehydrated and embedded. The paraffin sections were dewaxed, and 100 µl protease K was added to each section and incubated at 37 °C for 20 min. Sequentially, the sections were incubated in 2×SSC buffer for 3 min, dehydrated in graded alcohol (70%, 80%, 90%, 100%) for 2 min and air-dried. Then, the denaturing solution was preheated at 78 °C, and 100 µl denaturing solution was added to each section and incubated at 78 °C for 8 min. The alcohol gradient was repeated for dehydration and drying. The probe mix was prepared by mixing 15 µl of hybridization solution. Before the hybridization step, the probe mix was incubated at 73 °C for 30 min to clear and then at 73 °C for 5 min (denaturation). Later, sealed samples of the 10 µl probe mix were placed into a wet box and then incubated for 12–16 h at 37 °C for hybridization. After hybridization, the samples were washed twice with 2×SSC for 10 min at 37 °C and then with PBS for 10 min at RT. After incubating with 100 µl blocking buffer (0.5% Blocking Reagent/0.1 M TBS) for 15 min, the samples were reacted with the antibody in blocking buffer at RT for 2 h. After rinsing with PBS, 20 µl BCIP/NBT was added to each section at RT for 20–30 min for color development. Finally, Nuclear Fast Red solution was added to stain nuclei, slides were mounted, and images were captured.

Transmission electron microscopy (TEM)

The caudal epididymis from adult mice was placed in 500 µl PBS and incubated at 37 °C for 15 min. After centrifugation at 1500×g for 10 min, the supernatant was discarded, and 0.5% glutaraldehyde was added slowly to fix the sperm. The samples were incubated at 4 °C for 10 min and centrifuged at 1500×g for 15 min, and the supernatant was discarded. After the sperm were fixed in 2.5% glutaraldehyde at 4 °C overnight, they were processed by Lilai Biomedicine Experiment Center (Chengdu, China) as previously described [59]. The TEM protocol of the testis was to directly place the testis tissue in 2.5% glutaraldehyde, and the subsequent protocol was the same as above. All images were captured via a JEOL JM-1400Plus electron microscope (Tokyo, Japan) at 6000× and 12,000× magnification.

Histological, oil red O, immunofluorescence (IF) and TUNEL staining

Testis and epididymis samples were fixed in 4% paraformaldehyde (PFA) for 4 h at 4 °C as described previously [60] and dehydrated by 30, 50, 70, 95 and 100% ethanol for 4 h at each concentration gradient. After embedding in paraffin, the samples were cut into 4 µm sections. Rehydrated sections were stained with H&E and observed by a Nikon Eclipse E200 Microscope (Tokyo, Japan). For oil red O staining, PTMCs were fixed with 4% PFA for 10 min, rinsed with PBS, treated with 60% isopropanol for 20 s, and treated with oil red working solution (Servicebio, G1015) in the dark for 30 min. After removing the staining solution, 60% isopropanol quickly differentiated for 5 s. After washing the cells with ddH$_2$O, hematoxylin stained the nuclei, and after washing with ddH$_2$O, glycerol gelatin for sealing and observation with microscope. For IF analysis, tissue sections were deparaffinized and rehydrated and then boiled in 10 mM sodium citrate (pH 6.0) for 20 min for antigen retrieval. After blocking with 10% donkey serum for 1 h at RT, the sections were incubated with primary antibodies overnight at 4 °C. On the next day, the sections were washed three times in PBS, incubated with secondary antibodies for 2 h at RT in the dark and then washed three times in PBS. Finally, Hoechst 33,342 was added to the sections for 1 min. The sections were mounted in 50% glycerol before being examined under a Leica microscope. All antibodies are listed in Supplementary Table S1. For TUNEL staining, tissue sections were deparaffinized, rehydrated, subjected to antigen retrieval, and blocked, and then apoptotic cells were detected via a one-step TUNEL apoptosis assay kit (Beyotime, C1089) according to the manufacturer's instructions. The follow-up experiments were the same as those used for immunofluorescence. For IF staining of cultured PTMCs, cultured PTMCs were fixed in 4% PFA for 10 min at RT, washed three times with PBS and permeabilized with 0.1% Tween-20 for 1 h. After treatment with 10% donkey serum to block nonspecific staining, ACTA2 and DAPI were applied and incubated at 4 °C overnight, and then Alexa Fluor 488 antibody was applied to detect PTMCs. All images were captured using a confocal microscope.

Whole-mount immunostaining

EdU (RiboBio, Guangzhou, China) was injected intraperitoneally into mice at a dose of 50 mg/kg body weight. testes were collected 2 h after EdU injection. Seminiferous tubules were disentangled from mouse testes and fixed in 4% PFA at 4 °C for 4 h. After washing with PBS, seminiferous tubules were treated in PBS with 0.2% NP-40 for 20 min and dehydrated stepwise through a methanol series (25, 50, 75 and 100% methanol) in PBS containing 0.1% Tween 20 (PBST)

on ice. After rehydration in PBST for 30 min, tubules were incubated in blocking buffer (1% BSA and 4% donkey serum in PBST) for 1 h and incubated with primary antibodies diluted in blocking buffer at 4 °C overnight. After washing in PBST, tubules were incubated with secondary antibodies at RT for 2 h. Before EdU detection, IF staining was performed on Lin28 cells. Then, EdU was detected according to the manufacturer's instructions of the Cell-Light™ Edu Apollo 567 In Vivo Kit (RiboBio, C10310). A STELLARIS 5 SR confocal microscope (Leica) was used to image the samples.

In vitro fertilization and embryo culture

The in vitro fertilization (IVF) procedure was performed as described previously [59]. Briefly, epididymal sperm were collected from 9-month-old *Pnliprp2*$^{+/-}$ and *Pnliprp2*$^{-/-}$ male mice ($n=3$) and incubated in HTF medium for 1 h for capacitation. Cumulus-oocyte complexes (COCs) were collected from the oviduct ampullae of CD-1 female mice. Cumulus-free oocytes were inseminated with capacitated sperm and incubated with HTF medium at 37 °C in 5% CO_2. At 4 h postfertilization, oocytes were washed with HTF medium and cultured with KSOM medium in an incubator. The proportions of zygotes, 2-cell embryos, and blastocysts were assessed at 6, 24 and 96 h postfertilization, respectively.

Real-time quantitative PCR (qRT−PCR)

Total RNA was isolated using TRIzol reagent. After removing genomic DNA, RNA was reverse transcribed into cDNA using GenStar First-Strand cDNA Synthesis Mix with gDNA Remover (Beijing, China). qRT–PCR was performed with a TransStar green qPCR Supermix kit with 4 replicates per sample in an ABI Prism 7500 real-time fluorescence quantitative system (CA, USA). The cycle threshold (Ct) value was the average of four replicates, and relative gene expression was analyzed based on the $2^{-\Delta\Delta Ct}$ method. All the primers are listed in Table S3.

Coculture of PTMCs and THY1$^+$ testicular cells

The PTMCs were isolated from 6-month-old *Pnliprp2*$^{-/-}$ and control mice. The PTMC isolation protocol was adopted from Chen et al. [61]. Testes from adult mice were stripped of their tunica albuginea, digested with 1 mg/mL collagenase type IV and 1 mg/mL deoxyribonuclease (DNase) in Hank's balanced salt solution (HBSS) at 34 °C in a water bath for 15 min and washed 3 times with HBSS to remove interstitial cells. The remaining seminiferous tubules were further digested with 1 mg/mL collagenase type IV and 1 mg/mL DNase in HBSS for 20 min at 34 °C to release PTMCs and other cells. The digest was allowed to sediment at 4 °C for

5 min, and the supernatant was collected. The cells were pelleted at 4 °C, centrifuged for 7 min at 600 g and resuspended in 1 mL DMEM/Ham's F12 (DMEM/F12). A mixture of 10^8 cells was resuspended in DMEM/F12, applied to the top of a Percoll step gradient and centrifuged at 4 °C for 20 min at 800 g. The Percoll gradient solutions were prepared by mixing Percoll solution with DMEM/F12 to produce final solutions differing by 5% from 20 to 60% Percoll. One milliliter of each Percoll-DMEM/F12 solution was added to a 15-mL tube to obtain a 9-layer step gradient. After centrifugation, most PTMCs were located at the 35%/40% Percoll interface. To isolate THY1$^+$ testicular cells, testes from 5-day-old B6/129 mice were stripped of their tunica albuginea, placed in 2 ml HBSS and then pipetted five times to dissociate the tubules. After washing twice with HBSS, 10 ml of TE and 1 mg/ml DNase were added, and tubules were incubated at 37 °C to obtain a suspension of single cells. FBS (10%) was added to block the trypsin, and the solution was transferred to a 40 µm mesh cell strainer to filter out undigested tissue fragments. Cells were then washed twice with HBSS and pelleted by centrifugation at 600 g at 4 °C for 7 min. The cell concentration was adjusted to 10^8 cells in 180 µl DPBS, mixed with 20 µl THY1 antibody-linked magnetic microbeads, and incubated on ice for 40 min. THY1-positive cells were selected magnetically using MACS columns and a separator (Miltenyi BioTec). The isolated PTMCs were cultured in 12-well plates in 1 mL DMEM/F12 and 10% charcoal-stripped FBS for 48 h and then cocultured with THY1$^+$ spermatogonia (2×10^6) for qRT−PCR or immunostaining.

Untargeted lipid metabolism analysis

Seven testes were removed from both 5-week-old *Pnliprp2*$^{+/-}$ and *Pnliprp2*$^{-/-}$ mice, placed into liquid nitrogen for quick freezing and transferred to dry ice. Then, they were mailed to Shanghai Zhongke New Life Biotechnology Co., Ltd. for determination. The samples were pretreated, separated using a UHPLC Nexera LC-30A ultrahigh-performance liquid chromatography system, and finally analyzed by mass spectrometry using a Q Exactive plus mass spectrometer (Thermo Scientific™). LipidSearch software version 4.1 (Thermo Scientific) was used for peak identification, lipid identification (secondary identification), peak extraction, peak alignment, and quantitative processing. The main parameters were as follows: precursor tolerance: 5 ppm, product tolerance: 5 ppm, and product ion threshold: 5%. The obtained data were extracted, and lipid molecules with RSD > 30% were deleted. For the data extracted from LipidSearch, the lipid molecules with deletion values > 50% in the group were deleted, and the total peak area of the data was normalized. SIMCA-P 14.1 software (Umetrics, Umea, Sweden) was used for pattern recognition. After the data were preprocessed by Pareto scaling, multidimensional

statistical analysis was carried out, including unsupervised principal component analysis (PCA), supervised exclusive least squares discriminant analysis (PLS-DA) and orthogonal partial least squares discriminant analysis (OPLS-DA). Single-dimensional statistical analysis included Student's t test and variance multiple analysis. R software was used to draw volcano maps, perform hierarchical cluster analysis, and perform correlation analysis.

Single-cell RNA sequencing

Preparation of cell suspensions

Testes from 4-month-old *Pnliprp2*$^{+/-}$ and *Pnliprp2*$^{-/-}$ mice (n = 2) were collected in ice-cold PBS, and the tunica albuginea was removed using forceps. Testes were digested with 5 ml trypsin enzyme for 5 min at 37 °C, and 1 ml of 1 mg/ml DNase I was added. The samples were pipetted, and this operation was performed until the testis was digested into single cells. Cell masses were abandoned by 40 μm cell strainers. The single-cell suspension was pelleted by centrifugation at 400 × g for 5 min and resuspended in 5 ml PBS containing 0.4% BSA.

Single-cell library preparation and sequencing

scRNA-seq libraries were generated using the 10 × Genomics Chromium Controller Instrument and Chromium Single Cell 3' V3 Reagent Kits (10 × Genomics, Pleasanton, CA). Briefly, cells were concentrated to 1000 cells/μl, and approximately 15,000 cells were loaded into each channel to generate single-cell gel bead-in-emulsions (GEMs), which resulted in the expected mRNA barcoding of more than 6,000 single cells for each sample. After the RT step, GEMs were broken, and barcoded cDNA was purified and amplified. The amplified barcoded cDNA was fragmented, A-tailed, ligated with adaptors and index PCR amplified. The final libraries were quantified using the Qubit 2.0 A High Sensitivity DNA assay (Thermo Fisher Scientific) and the size distribution of the libraries were determined using a High Sensitivity DNA chip on a Bioanalyzer 2100 (Agilent). All libraries were sequenced by NovaSeq 6000 (Illumina, San Diego, CA) on a 150 bp paired-end run.

Primary single-cell data analysis

We applied fastq with default parameter filtering of the adaptor sequence and removed the low-quality reads to achieve clean data. Then, alignment, filtering, barcode counting and UMI quantification for determining gene transcript counts per cell (generating a gene-barcode matrix), quality control, clustering and statistical analysis were performed by aligning reads to the mm10 genome using the CellRanger count command. Cells containing fewer than 200 expressed genes and mitochondrial genes were removed from the expression table but used for cell expression regression to avoid the effect of the cell status for clustering analysis and marker analysis of each cluster. The Seurat package (version: 4.0.2) was used for cell normalization and regression based on the expression table according to the UMI counts of each sample and percent of mitochondria rate to obtain the scaled data. PCA was constructed based on the scaled data with all highly variable genes, and the top 10 principals were used for tSNE construction. Utilizing the graph-based cluster method, we acquired the unsupervised cell cluster result based on the PCA top 20 principal, and we calculated the marker genes by the FindAllMarkers function with the Wilcoxon rank sum test algorithm under the following criteria: 1. Log2FC > 0.25; 2. *P* value < 0.05; 3. min.pct > 0.1. We applied single-cell trajectory analysis utilizing Monocle2 (http://cole-trapnell-lab.github.io/monocle-release) using DDR-Tree and default parameters. Before Monocle analysis, we selected marker genes of the Seurat clustering result, and raw expression counts of the cell passed filtering. Cell communication between cell types was analyzed by CellChat R Package and Secreted Signaling of interaction in *CellChatDB*. Mouse serves as a receptor ligand library.

Statistical analysis

The data were statistically analyzed with one-way ANOVA and LSD test using IBM SPSS software (IL, USA). All quantitative data are presented as the mean ± standard error for at least 3 biological replicates. Differences between means were considered significant at *P* < 0.05.

reasonable request. Single-cell RNA-seq datasets have been uploaded to NCBI (BioProject: PRJNA898878).

Declarations

Conflicts of interest These authors declare that they have no competing interests.

Ethical approval Animal experiments were performed in accordance with the Guide for the Care and Use of Laboratory Animals and were approved by the Animal Welfare and Ethics Committee at the Northwest Institute of Plateau Biology, Chinese Academy of Sciences (approval code: hwipb012).

Consent for publication Not applicable.

References

1. Griswold MD (2016) Spermatogenesis: the commitment to Meiosis. Physiol Rev 96:1–17
2. Maekawa M, Kamimura K, Nagano T (1996) Peritubular myoid cells in the testis: their structure and function. Arch Histol Cytol 59:1–13
3. Fernandez D et al (2008) Identification and characterization of myosin from rat testicular peritubular myoid cells. Biol Reprod 79:1210–1218
4. Russell LD, de Franca LR, Hess R, Cooke P (1995) Characteristics of mitotic cells in developing and adult testes with observations on cell lineages. Tissue Cell 27:105–128
5. Chen LY, Willis WD, Eddy EM (2016) Targeting the Gdnf Gene in peritubular myoid cells disrupts undifferentiated spermatogonial cell development. Proc Natl Acad Sci U S A 113:1829–1834
6. Zhou R et al (2019) The roles and mechanisms of Leydig cells and myoid cells in regulating spermatogenesis. Cell Mol Life Sci 76:2681–2695
7. Kanatsu-Shinohara M et al (2003) Long-term proliferation in culture and germline transmission of mouse male germline stem cells. Biol Reprod 69:612–616
8. Meng X et al (2000) Regulation of cell fate decision of undifferentiated spermatogonia by GDNF. Science 287:1489–1493
9. Creemers LB et al (2002) Transplantation of germ cells from glial cell line-derived neurotrophic factor-overexpressing mice to host testes depleted of endogenous spermatogenesis by fractionated irradiation. Biol Reprod 66:1579–1584
10. Davis JT, Ong DE (1995) Retinol processing by the peritubular cell from rat testis. Biol Reprod 52:356–364
11. Welsh M, Saunders PT, Atanassova N, Sharpe RM, Smith LB (2009) Androgen action via testicular peritubular myoid cells is essential for male fertility. FASEB J 23:4218–4230
12. Ademi H et al (2022) Deciphering the origins and fates of steroidogenic lineages in the mouse testis. Cell Rep 39:110935
13. Clark AM, Garland KK, Russell LD (2000) Desert hedgehog (Dhh) gene is required in the mouse testis for formation of adult-type Leydig cells and normal development of peritubular cells and seminiferous tubules. Biol Reprod 63:1825–1838
14. Chiarenza C, Filippini A, Tripiciano A, Beccari E, Palombi F (2000) Platelet-derived growth factor-BB stimulates hypertrophy of peritubular smooth muscle cells from rat testis in primary cultures. Endocrinology 141:2971–2981
15. Rebourcet D et al (2014) Sertoli cells control peritubular myoid cell fate and support adult Leydig cell development in the prepubertal testis. Development 141:2139–2149
16. Cool J, Carmona FD, Szucsik JC, Capel B (2008) Peritubular myoid cells are not the migrating population required for testis cord formation in the XY gonad. Sex Dev 2:128–133
17. Uchida A et al (2020) Development and function of smooth muscle cells is modulated by Hic1 in mouse testis. Develop. https://doi.org/10.1242/dev.185884
18. Qian Y et al (2013) Lgr4-mediated Wnt/beta-catenin signaling in peritubular myoid cells is essential for spermatogenesis. Development 140:1751–1761
19. Giller T, Buchwald P, Blum-Kaelin D, Hunziker W (1992) Two novel human pancreatic lipase related proteins, hPLRP1 and hPLRP2. Differences in colipase dependence and in lipase activity. J Biol Chem 267:16509–16516
20. Mahan JT, Heda GD, Rao RH, Mansbach CM 2nd (2001) The intestine expresses pancreatic triacylglycerol lipase: regulation by dietary lipid. Am J Physiol Gastrointest Liver Physiol 280:G1187-1196
21. Amara S et al (2010) Lipolysis of natural long chain and synthetic medium chain galactolipids by pancreatic lipase-related protein 2. Biochim Biophys Acta 1801:508–516
22. Gilleron M et al (2016) Lysosomal lipases PLRP2 and LPLA2 process mycobacterial multi-acylated lipids and generate t cell stimulatory antigens. Cell Chem Biol 23:1147–1156
23. Gao Y et al (2019) Pancreatic lipase-related protein 2 is responsible for the increased hepatic retinyl ester hydrolase activity in vitamin a-deficient mice. Febs j 286:4232–4244
24. Pang W et al (2011) The mPlrp2 and mClps genes are involved in the hydrolysis of retinyl esters in the mouse liver. J Lipid Res 52:934–941
25. Lowe ME, Kaplan MH, Jackson-Grusby L, D'Agostino D, Grusby MJ (1998) Decreased neonatal dietary fat absorption and T cell cytotoxity in pancreatic lipase-related protein 2-deficient mice. J Biol Chem 273:31215–31221
26. Lowe ME (2000) Properties and function of pancreatic lipase related protein 2. Biochimie 82:997–1004
27. Xu L, Huang HJ, Zhou X, Liu CW, Bao YY (2017) Pancreatic lipase-related protein 2 is essential for egg hatching in the brown planthopper. Nilaparvata lugens Insect Mol Biol 26:277–285
28. Sias B et al (2005) Cloning and seasonal secretion of the pancreatic lipase-related protein 2 present in goat seminal plasma. Biochim Biophys Acta 1686:169–180
29. Chen SR, Liu YX (2016) Myh11-Cre is not limited to peritubular myoid cells and interaction between Sertoli and peritubular myoid cells needs investigation. Proc Natl Acad Sci USA 113:E2352
30. Corliss BA et al (2019) Myh11 Lineage Corneal Endothelial Cells and ASCs Populate Corneal Endothelium. Invest Ophthalmol Vis Sci 60:5095–5103
31. Tateno H et al (2013) Ca2+ ionophore A23187 can make mouse spermatozoa capable of fertilizing in vitro without activation of cAMP-dependent phosphorylation pathways. Proc Natl Acad Sci USA 110:18543–18548
32. Wang YQ, Batool A, Chen SR, Liu YX (2018) GATA4 is a negative regulator of contractility in mouse testicular peritubular myoid cells. Reproduction 156:343–351
33. Li L et al (2017) Single-cell RNA-Seq analysis maps development of human germline cells and gonadal niche interactions. Cell Stem Cell 20:858–873
34. Davis JT, Bridges RB, Coniglio JG (1966) Changes in lipid composition of the maturing rat testis. Biochem J 98:342–346
35. Lenzi A, Picardo M, Gandini L, Dondero F (1996) Lipids of the sperm plasma membrane: from polyunsaturated fatty acids considered as markers of sperm function to possible scavenger therapy. Hum Reprod Update 2:246–256
36. Cross NL (1994) Phosphatidylcholine enhances the acrosomal responsiveness of human sperm. J Androl 15:484–488

37. Rana AP, Misra S, Majumder GC, Ghosh A (1993) Phospholipid asymmetry of goat sperm plasma membrane during epididymal maturation. Biochim Biophys Acta 1210:1–7

38. Infante JP, Huszagh VA (1985) Synthesis of highly unsaturated phosphatidylcholines in the development of sperm motility: a role for epididymal glycerol-3-phosphorylcholine. Mol Cell Biochem 69:3–6

39. Masaki H et al (2017) Long-chain fatty acid triglyceride (TG) metabolism disorder impairs male fertility: a study using adipose triglyceride lipase deficient mice. Mol Hum Reprod 23:452–460

40. Gorga A et al (2017) PPARγ activation regulates lipid droplet formation and lactate production in rat Sertoli cells. Cell Tissue Res 369:611–624

41. Agarwal AK et al (2017) Metabolic, reproductive, and neurologic abnormalities in Agpat1-null mice. Endocrinology 158:3954–3973

42. Hermo L et al (2008) Alterations in the testis of hormone sensitive lipase-deficient mice is associated with decreased sperm counts, sperm motility, and fertility. Mol Reprod Dev 75:565–577

43. Ebihara C et al (2015) Seipin is necessary for normal brain development and spermatogenesis in addition to adipogenesis. Hum Mol Genet 24:4238–4249

44. Virtanen I et al (1986) Peritubular myoid cells of human and rat testis are smooth muscle cells that contain desmin-type intermediate filaments. Anat Rec 215:10–20

45. Xiao X, Ross LE, Sevilla WA, Wang Y, Lowe ME (2013) Porcine pancreatic lipase related protein 2 has high triglyceride lipase activity in the absence of colipase. Biochim Biophys Acta 1831:1435–1441

46. Alves BN et al (2009) Pancreatic lipase-related protein 2 (PLRP2) induction by IL-4 in cytotoxic T lymphocytes (CTLs) and reevaluation of the negative effects of its gene ablation on cytotoxicity. J Leukocyte Biol 86:701–712

47. Ding Z et al (2022) The suppression of pancreatic lipase-related protein 2 ameliorates experimental hepatic fibrosis in mice. Bba-Mol Cell Biol L 1867:1591

48. de Rooij DG, Russell LD (2000) All you wanted to know about spermatogonia but were afraid to ask. J Androl 21:776–798

49. Richardson LL, Kleinman HK, Dym M (1995) Basement membrane gene expression by Sertoli and peritubular myoid cells in vitro in the rat. Biol Reprod 52:320–330

50. Siu MK, Cheng CY (2008) Extracellular matrix and its role in spermatogenesis. Adv Exp Med Biol 636:74–91

51. Lord T, Nixon B (2020) Metabolic changes accompanying spermatogonial stem cell differentiation. Dev Cell 52:399–411

52. Kanatsu-Shinohara M et al (2016) Myc/Mycn-mediated glycolysis enhances mouse spermatogonial stem cell self-renewal. Genes Dev 30:2637–2648

53. Boussouar F, Benahmed M (2004) Lactate and energy metabolism in male germ cells. Trends Endocrinol Metab 15:345–350

54. Regueira M et al (2018) Apoptotic germ cells regulate Sertoli cell lipid storage and fatty acid oxidation. Reproduction 156:515–525

55. Holdcraft RW, Braun RE (2004) Androgen receptor function is required in Sertoli cells for the terminal differentiation of haploid spermatids. Development 131:459–467

56. Tripiciano A, Palombi F, Ziparo E, Filippini A (1997) Dual control of seminiferous tubule contractility mediated by ETA and ETB endothelin receptor subtypes. FASEB J 11:276–286

57. Johnson K, Ross L, Miller R, Xiao X, Lowe ME (2013) Pancreatic lipase-related protein 2 digests fats in human milk and formula in concert with gastric lipase and carboxyl ester lipase. Pediatr Res 74:127–132

58. Tanphaichitr N, Hansen C (1994) Production of motile acrosome-reacted mouse sperm with nanomolar concentration of calcium ionophore A23187. Mol Reprod Dev 37:326–334

59. Tao HP et al (2022) Paternal hypoxia exposure impairs fertilization process and preimplantation embryo development. Zygote 30:48–56

60. Yan RG, Li BY, Yang QE (2020) Function and transcriptomic dynamics of Sertoli cells during prospermatogonia development in mouse testis. Reprod Biol 20:525–535

61. Chen L-Y, Brown PR, Willis WB, Eddy EM (2014) Peritubular Myoid Cells Participate in Male Mouse Spermatogonial Stem Cell Maintenance. Endocrinology 155:4964–4974